Konya Mühendislik Bilimleri Dergisi., c. 13, s. 4, 1107-1136, 2025
Konya Journal of Engineering Sciences v. 13, n. 4, 1107-1136, 2025
ISSN: 2667-8055 (Electronic)
DOI: 10.36306/konjes.1674751

METAHEURISTIC METHODS OPTIMIZED HSMC CONTROL OF A MULTI DOF HAND AND WRIST REHABILITATION ROBOT DESIGN

[1,*] **Musa MARUL**, [2] **Nurhan GÜRSEL ÖZMEN**

[1] *Artvin Çoruh University, Borçka Acarlar Vocational School, Electronics and Automation Department, Artvin, TÜRKİYE*
[2] *Karadeniz Technical University, Mechanical Engineering Department, Trabzon, TÜRKİYE*
[1] akumusa@artvin.edu.tr, [2] gnurhan@ktu.edu.tr

Highlights

- A novel HSMC controller for multi DOF robot is proposed.
- PSO and DE for optimization of HSMC and HPID.
- A successful trajectory tracking, and minimum errors are obtained.

Graphical Abstract

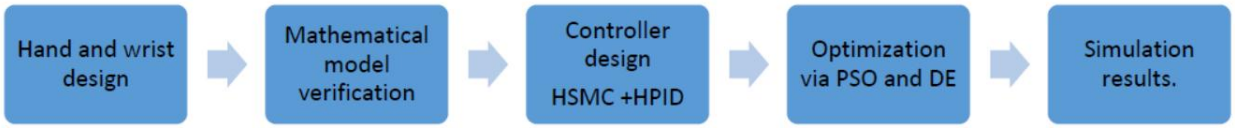

Flowchart of the proposed method

***Corresponding Author:** Musa MARUL, akumusa@artvin.edu.tr

Konya Mühendislik Bilimleri Dergisi., c. 13, s. 4, 1107-1136, 2025
Konya Journal of Engineering Sciences v. 13, n. 4, 1107-1136, 2025
ISSN: 2667-8055 (Electronic)
DOI: 10.36306/konjes.1674751

METAHEURISTIC METHODS OPTIMIZED HSMC CONTROL OF A MULTI DOF HAND AND WRIST REHABILITATION ROBOT DESIGN

[1,*] Musa MARUL, [2] Nurhan GÜRSEL ÖZMEN

[1] *Artvin Çoruh University, Borçka Acarlar Vocational School, Electronics and Automation Department, Artvin, TÜRKİYE*
[2] *Karadeniz Technical University, Mechanical Engineering Department, Trabzon, TÜRKİYE*
[1] akumusa@artvin.edu.tr , [2] gnurhan@ktu.edu.tr

(Received: 12.04.2025; Accepted in Revised Form: 24.07.2025)

ABSTRACT: Rehabilitation is a process that aims to restore individuals to full functionality following an injury or illness that has compromised their ability to perform daily activities. A significant challenge in addressing these needs is the selection of robotic devices that can adequately respond to the complex requirements of rehabilitation. This study presents a simulation study for the position control of the wrist and fingers using Hierarchical Sliding Mode Control (HSMC) that is optimized via metaheuristic algorithms. A novel hierarchical approach is applied that is optimized with Particle Swarm Optimization (PSO) and Differential Evolution (DE) algorithms. The model was simulated under disturbances to track the desired trajectory. Simulation results are compared with Hierarchical PID controller results. The findings demonstrate that HSMC-based control effectively improve trajectory tracking, reducing mean absolute and normalized root mean square (NRMS) errors compared to HPID controllers. The proposed approach shows promising potential for real implementation, enhancing the efficiency of rehabilitation devices.

Keywords: *Rehabilitation Robot, Hierarchical Sliding Mode Control (HSMC), Hand Rehabilitation, Particle Swarm Optimization (PSO), Differential Evolution (DE)*

1. INTRODUCTION

The elderly population of the world is increasing, bringing new aids for their decreasing physical capabilities due to stroke or similar diseases. Additionally, injuries to the upper limbs, including the hands and arms, may occur after various accidents and natural disasters. These patients require prompt and comprehensive rehabilitation to regain their lost abilities and resume their normal daily activities. Advancements in engineering and robotic technology, particularly in the context of rehabilitation, have shown remarkable progress. However, the current state of these technologies are still in progress. The existing models, which are limited in their range of motion or depend on a single actuator type, represent only a fraction of the full scope of human hand and wrist capabilities. Systems with limited degrees of freedom are inadequate in replicating the full range of motion of a human hand and wrist. Research on rehabilitation techniques to enhance motor and cognitive function in patients with paralysis or muscle weakness is ongoing [1]. Rehabilitation methods vary based on the type of disease and patient characteristics [2, 3]. A patient-centred approach is prioritized over a disease-centred approach in rehabilitation, emphasizing personalized movement patterns. Consequently, the design of rehabilitation equipment and movement selection should involve physiotherapists and rehabilitation specialists[4, 5] Instead of focusing solely on time-based exercises, rehabilitation should prioritize achieving sufficient strength and mobility for each patient [6]. Experimental and clinical studies incorporate movement patterns and joint mobilization exercises prescribed by physiotherapists. Therapeutic exercises, tailored for disease-specific treatment, aim to enhance limb strength, endurance, and mobility. These exercises are categorized into passive, active, active-assisted, resistance, and isokinetic exercises.

Experimental and clinical studies incorporate movement patterns and joint mobilization exercises prescribed by physiotherapists. Therapeutic exercises, tailored for disease-specific treatment, aim to

***Corresponding Author:** Musa MARUL, akumusa@artvin.edu.tr

enhance limb strength, endurance, and mobility. These exercises are categorized into passive, active, active-assisted, resistance, and isokinetic exercises.

Rehabilitation of the hand and wrist poses significant challenges due to the anatomical complexity of the region, characterized by its high degree of mobility. The wearable exoskeletons, with the support device offers compact design. To date, research has been conducted on the use of functional electrical stimulation (FES) based hand rehabilitation devices, virtual reality (VR)-based stroke rehabilitation and telerehabilitation, and finger function [7]. Among functional movements, hand opening is the most frequently used, followed by grasping and wrist movement [8].

Hand rehabilitation is a process that consists of holding the hand in a fixed position (immobilization), improving the range of motion, stretching, and strengthening. Rehabilitation robots should have a design that the patient can use in their daily life during treatment, and in the period after treatment is completed. The design of rehabilitation robots must be comfortable, easy to assemble and disassemble, and cost effective [9, 10]. The mechanisms should also be adjustable and ergonomic [11]. They should follow a trajectory. For this reason, applications are often defined by a trajectory or a specific exercise [12, 13].

Different types of rehabilitation robots are given in the literature [14]. The classification process considers many parameters, such as design, type of motion, degrees of freedom, material, drive type, and drive train. A classification based on these characteristics is shown in Table 1. The first of these classifications is exoskeleton hand rehabilitation robots [15-28]. The second classification group consists of end-effector hand rehabilitation robots [29-46].

Robotic devices developed for hand rehabilitation still have shortcomings today. While the rehabilitation process with traditional rigid systems produces successful results for the individual user, the same mechanism may not produce successful results for different patients [47]. Clinical applications of the developed devices must be widespread [48].

In general, hand rehabilitation robots are built as independent, single actuator or partial examination of the hand to perform standardized hand movements. The existing devices either are heavy, bulky, or only accommodate a limited range of motions and maximum contact forces [15, 49-52]. There are a limited number of robot designs with multiple degrees of freedom. The main reason is that it is too complex to precisely design and develop those systems. Moreover, nonlinear control techniques are needed, which are more difficult to apply [53].

There are mainly three different drive mechanisms for hand exoskeletons to deliver a compact and lightweight force that are linkage-based, cable-driven, and soft actuator. Each has advantages and disadvantages like the linkage-based mechanism which offers the highest rigidity and linear force transmission, but has a complex structure, is heavy, and produces high stresses on supporting elements [15, 50, 51]. Cable-driven mechanisms have high rigidity, are far more lightweight, have linear force transmission, and enable to put actuators apart from the device. On the other hand, friction along the transmission is a serious problem. Moreover, the placement of cables problem should be resolved [49, 54-57]. Soft-actuator-based or shape memory alloy-based mechanisms are lightweight, have high compliance, low inherent stiffness, and are safer than the others. However, it has limited degrees of freedom, is less efficient, and may produce shear forces on joints [52, 58, 59].

A good control strategy is necessary for the correct tracking of prescribed motions by the robotic device. There are studies in the literature about commonly used PID controllers for the tracking performance of hand and wrist robots in the literature [60]. Most of them have one, two or three DOFs. In literature, Widhiada et al. [54] studied a multi-fingered robot hand control. They designed an advanced PID control with automatic adjustment to achieve a fast steady-state response and reduce convergence time [61].

Table 1. Overview of existing hand rehabilitation robots [14]

Groups	Researchers	Actuated DoF	Driving Modes	Control Strategies	Force Transmission Mode
The exoskeleton hand rehabilitation robots	J. Iqbal et al.	4	Motor	Preset	Link
	D. Leonardis et al.	5	Motor	Preset	Link
	R. Conti et al.	4	Motor	Preset	Rope + Connecting rod
	S. Kim et al.	1	Motor	Preset	Link
	Decker et al.	5	Motor	Preset	Link
	I. Jo et al.	5	Motor	Preset	Link
	Sale et al.	4	Motor	Preset	Cable+ Chain
	F. Zhang et al.	6	Motor	Preset	Cable + Link
	A. Lince et al.	1	Motor	EMG	Cable + Link
	A. Bataller et al.	1	Motor	Preset	Link
	I. Jo et al.	1	Motor	Preset	Spring + Link
	D. Marconi et al.	5	SEA	Force Control	Link
The end-effector hand rehabilitation robots	Haghshenas J. M. et al.	3	Hybrid pneumatic	Preset	Pneumatic artificial muscle
	Polygerinos, P. et al.	5	Hydraulic	Preset	Rubber Return Spring
	Diftler, M.A. et al.	3	Motor	Force Control	Tendon/Cable-pulley
	Fischer, H.C et al.	5	Motor	Preset	Cable
	H. K. Yap et al.	5	Pneumatic	EMG	Flexible Actuators
	Y. Park et al.	3	Motor	Force Control	Cable
	D. Marconi et al.	5	SEA	Force Control	Link
	B.W. K. Ang et al.	5	Pneumatic	EMG	Flexible Actuators
	B. B. Kang et al.	2	Motor	Force feedback control	Cable
	D. Popov et al.	4	Motor	Preset	Tendon
The end-effector hand rehabilitation robots	L. Randazzo et al.	5	Motor	EEG	Artificial tendon
	Thielbar, K.O. et al.	5	Motor	Active task orientation	Tendon/Cable pulley
	Chua, M.C. et al.	4	Pneumatic	Force Control	Pneumatic artificial muscle
	M. Li et al.	5	Motor	EEG	Multi-Segment
	Butzer, T. et al	2	DC Motor	EMG	Spring blade
	Qiaoling Meng et al.	1	Motor	Force Control	Tendon
	Zhi Qiang Tang et al.	5	Pneumatic	EMG	Pneumatic artificial muscle
	M. Sierotowicz et al.	2	Motor	EMG	Tendon

Sliding-mode control (SMC) is seen as a suitable choice for rehabilitation robot tracking control compared to PID, because it is not sensitive to external interference [62, 63]. A robust sliding mode

controller is applied successfully to control a hand exoskeleton in [64]. On the other hand, for higher degrees of freedom systems, the generation of mathematical model becomes complex. To overcome the mathematical model development problem, a model-free adaptive fuzzy sliding-mode controller was proposed by Jalali et al [65]. They replaced the equivalent dynamic model in SMC with a fuzzy logic controller. In a recent study by Hu [66], an impedance sliding-mode control method based is introduced. The method relies on stiffness-scheduled law for the rehabilitation robot, and can be applied to both active and passive exercises during rehabilitation training. The study findings are satisfactory. The patients' recovery condition was taken into account rather than the existing studies by using an impedance sliding mode controller design in robot-assisted rehabilitation.

Apart from the studies in the literature, a multi DOF hand and wrist rehabilitation robot control is considered in this study. In this paper, the authors present the simulation results of the prototype design which reveals interesting properties to be studied in the future works. A novel Hierarchical Sliding Mode Controller is designed to control the passive tasks of hand and wrist system. In order to train the wrist and the fingers individually after a stroke or an accident, a simulation study is carried out in order to implement the real prototype. The system's performance is compared with a hierarchical PID controller. Moreover, the controller parameters were optimized using PSO and DE algorithms in order to serve for the best performing algorithm. This study is aimed to contribute to the field of rehabilitation robot applications.

The rest of the study continues with the controller design in section 2, which contains the HSMC and HPID settings for different optimization algorithms. In section 3, the findings of the study are presented with the discussions. Finally, conclusions are given in Section 4.

2. MATERIALS AND METHODS

The nonlinear mathematical model of the proposed rehabilitation robot with 18 degrees of freedom, is obtained by the simplified Lagrange method. Hand-wrist simulation exercises were performed according to the rehabilitation criteria between the limits of the human hand [67]. These criteria are given in Table 2.

2.1. Mathematical Modelling of the Mechanism

The biomechanical model of the hand takes into account the structure and degrees of freedom of the limb. The interphalangeal joints of the hand are the hinge joints between the phalanges of the fingers, and they provide flexion/extension. Proximal interphalangeal joints (PIP) and distal interphalangeal joints (DIP) joints have the similar structure in different sizes. The carpometacarpal joint (CMC) and metacarpophalangeal joints (MCP) have two degrees of freedom, both flexion/extension and abduction/adduction, however, in this study they are represented as single DOF. The wrist joint has two degrees of freedom, flexion/extension and abduction/adduction [68]. In the three-dimensional XYZ plane, where the radial/ulnar deviation of the wrist is taken into account, the wrist is represented by the ZY axis angle φ_1. The thumb trapeziometacarpal (TMC) joint, or, the base of the thumb, is also represented by the ZY axis as angle φ_2. The physical model of the studied hand showing is orientations is depicted in Figure 1. The mathematical model of the system is obtained by simplified Lagrange equation using kinetic and potential energy as in [69]. The effect of the muscles and tendons, and frictions were neglected for ease of solution.

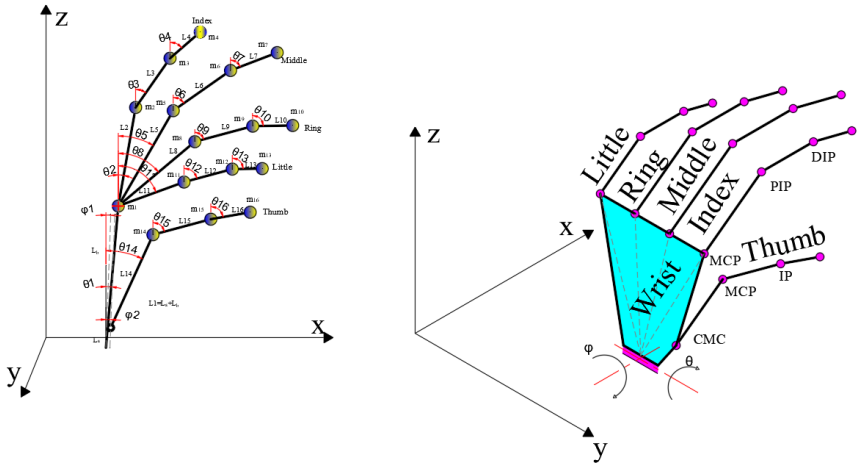

Figure 1. 18 DOF hand-wrist model

$$\frac{d}{dt}\left(\frac{\partial L}{\partial \dot{\theta}_i}\right)-\frac{\partial L}{\partial \theta_i}=\tau_i \ , i=1:16 \tag{1}$$

$$\frac{d}{dt}\left(\frac{\partial L}{\partial \dot{\varphi}_j}\right)-\frac{\partial L}{\partial \varphi_j}=\tau_j \ , \begin{cases} j:1\rightarrow \tau_{17} \\ j:2\rightarrow \tau_{18} \end{cases} \tag{2}$$

where, L is Lagrangian; $\theta_i,\theta_{ip},\dot{\theta}_i,\dot{\theta}_{ip},\ddot{\theta}_i,\ddot{\theta}_{ip}$, $i=1:16$ and $\varphi_j,\varphi_{jp},\dot{\varphi}_j,\dot{\varphi}_{jp},\ddot{\varphi}_j,\ddot{\varphi}_{jp}$, $j=1:2$ parameters represent the position, angular velocity and the acceleration vectors of of each joint i. τ_i (t) is the given torque vector at joints. The Lagrangian L can be represented as ,

$$L=T_i-V_i, \ i=1:16 \tag{3}$$

where T_i and V_i denote the kinetic and potential energies at each joint, respectively.

$$T_i=\frac{1}{2}m_i v_i^2 \rightarrow i=1:16, V_i=m_i g h_i \rightarrow i=1:16 \tag{4}$$

Substituting the equations into (1), dynamic equations of all digits and wrist can be obtained as below,

$$\begin{aligned} &\mathrm{M}_i(\theta)\ddot{\theta}+C_i(\theta,\dot{\theta})+G_i(\theta)=\tau_i \ , i=1:16 \\ &\mathrm{M}_j(\varphi)\ddot{\varphi}+C_j(\varphi,\dot{\varphi})+G_j(\varphi)=\tau_j \ , j=1:2 \end{aligned} \tag{5}$$

Here, the damping and the Coriolis effects are neglected. The final dynamic equations for each finger and for each joint are calculated according to the Lagrange formula. The mathematical expressions for each digit and joint are too large to add in this part. The formulas for the final two joints are given here.

The dynamic relations for the two-link thumb, the three-link fingers and the wrist are described in [70] explicitly.

$$\ddot{\theta}_{16} = \frac{\left(\tau_{16} + \frac{\partial L_T}{\partial \theta 16} - \begin{pmatrix} dfi1 + dfi2 + dtheta1 + dtheta14 + dtheta15 + dtheta16 \\ fi1 + fi2 + theta1 + theta14 + theta15 + theta16 \end{pmatrix}\right)}{m_{16} L^2_{16} (c^2\varphi_2 c^2\theta_{16} + s^2\theta_{16})} \tag{6}$$

$$\ddot{\varphi}_2 = \frac{\tau_{18} + \frac{\partial L_T}{\partial \varphi_2} - \begin{pmatrix} dfi1 + dfi2 + dtheta1 + dtheta14 + dtheta15 + dtheta16 \\ fi1 + fi2 + theta1 + theta14 + theta15 + theta16 \end{pmatrix}}{\left(\begin{array}{l} m_{14} L_{14}{}^2 \left(s^2\varphi_2 \, s^2 \, \theta_{14} + c^2\theta_{14} \right) \\ + m_{15} \left(\begin{array}{l} L_{14}{}^2 \left(c^2\theta_{14} c^2\varphi_2 + s^2\theta_{14} \right) + L_{15}{}^2 \left(c^2\theta_{15} c^2\varphi_2 + c^2\theta_{15} \right) \\ + L_{14} L_{15} \left(s^2\varphi_2 s\theta_{14} s\theta_{15} + c^2\varphi_2 c\theta_{14} c\theta_{15} + s^2\varphi_2 c\theta_{14} c\theta_{15} \right) \end{array} \right) \\ + m_{16} \left(\begin{array}{l} L_{14}{}^2 \left(s^2\varphi_2 \, s^2 \, \theta_{14} + c^2\theta_{14} \right) + L_{15}{}^2 \left(s^2\varphi_2 s^2\theta_{15} + c^2\theta_{15} \right) \\ + L_{16}{}^2 \left(s^2\varphi_2 s^2\theta_{16} + c^2\theta_{16} \right) \end{array} \right) \end{array} \right)} \tag{7}$$

Here, c is used for cosine and s for sine.

2.2. Controller Design

The nonlinear dynamics represented by (6-7) is fed to the system defining the position/velocity state by using nonlinear controllers as hierarchical sliding mode control (HSMC) and hierarchical proportional integral derivative control (HPID).

2.2.1.Hierarchical Sliding Mode Control (HSMC)

Sliding mode controllers are one of the most preferred methods due to their good performance in tracking disturbance trajectories in linear and nonlinear systems [10, 71-73] . It is a control system with a variable structure. Since the supervisory control of real systems is difficult, the control rules are changed according to predetermined rules. Hierarchical SMC is a specialization of sliding mode control for controlling multilevel dynamical systems or complex systems with many interacting subsystems. To control mathematical equations with multiple dynamic structures, sliding planes are defined for different subsystems and solved in a hierarchy [74]. The proposed HSMC algorithm used 10 steps to control the 18 DOF hand wrist model. First, the equations defining the position, velocity, and accelerations of the exoskeleton robot are decomposed and new variables are defined. A sliding surface is defined for each plane. The next step is to relate each layer to the others. Finally, in order to orient the system to the respective sliding plane, it is ensured that the system works stably and smoothly according to the Lyapunov stability principle.

SMC consists of two sections. The first goal is to create the sliding surface. This allows the system to reach a sliding surface by switching between stable or unstable trajectories and to reach the origin by sliding on this surface. This is the sliding plane,

$$S = C\xi + \dot{\xi} \tag{8}$$

Here $C\,(C > 0)$ is a positive coefficient. Ksi (ξ) is the time-dependent variable to be controlled.

In the second step, a new control variable is assigned. This control variable is the auxiliary sliding plane and replaces the main sliding planes. This sliding plane is defined as,

$$S_m = S \tag{9}$$

Lyapunov function is given as,

$$\dot{S}_m \leq 0 \tag{10}$$

This new equation is written into the main function of the second step of the SMC control method, and the stabilization stage is done. It is defined with the following equation,

$$V = -k_1 S_m - k_2 \tanh(S_m) \tag{11}$$

The $k\,(k > 0)$ are positive coefficients. The goal $V \leq 0$ is to meet the stabilization criterion. This function is also used as a cost function in optimization algorithms. When it is on the sliding surface, it behaves like a first-order system. This ensures that the system response reaches a desired value without overshoot. The general structure of HSMC is accomplished in **10 steps**. This situation is presented in Figure 2.

2.2.2 Hierarchical Proportional Integral Derivative Control (HPID)

The general PID controller creates a new signal closest to the desired value by taking the difference between the output and input values of a system as a reference. The tracking error e(t) is defined as

$$e(t) = r(t) - y(t) \tag{12}$$

r is the desired angle vector of joints; and *y* is the actual angle vector of joints. The PID controller parameters consisting of three terms Kp, Ki and Kd are determined by taking the input value u(t) produced in a system as a reference to the error input value e(t). These parameters are,

$$u(t) = K_p e(t) + K_i \int_0^t e(t)\,dt + K_d \frac{de(t)}{dt} \tag{13}$$

Kp represents proportional gain, Ki represents integral gain, and Kd represents derivative gain. Since PID control provides poor control in nonlinear systems, a Hierarchical PID (HPID) is proposed in this paper. HPID is a piecewise PID control method developed for the control of complex dynamical systems where the control is difficult, as in the case of HSMC method. The solution of HPID control is constructed in ten steps.

The overall controller design is shown in Figure 2. The Simulink model consists of steps from 1 to 10.

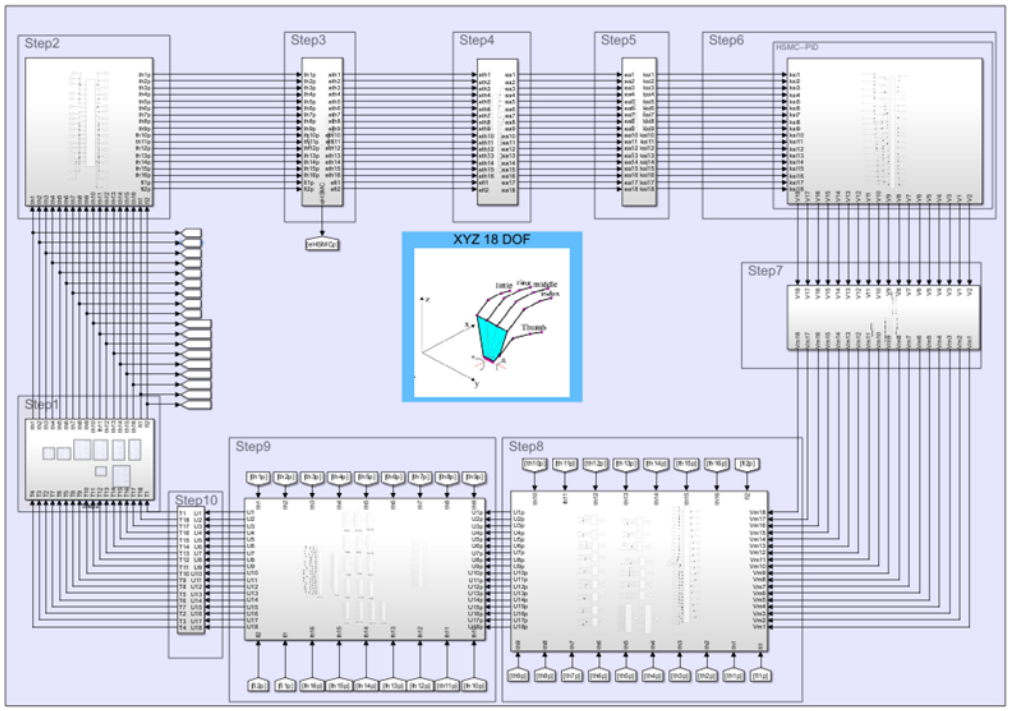

Figure 2. Simulink model of the entire hand and wrist system

Step 1 in the Simulink environment contains the acceleration equations for 18 DOF system. It is the part that contains the basic mathematical model of each joint. The inner Simulink model structure for the is given in Figure 3.

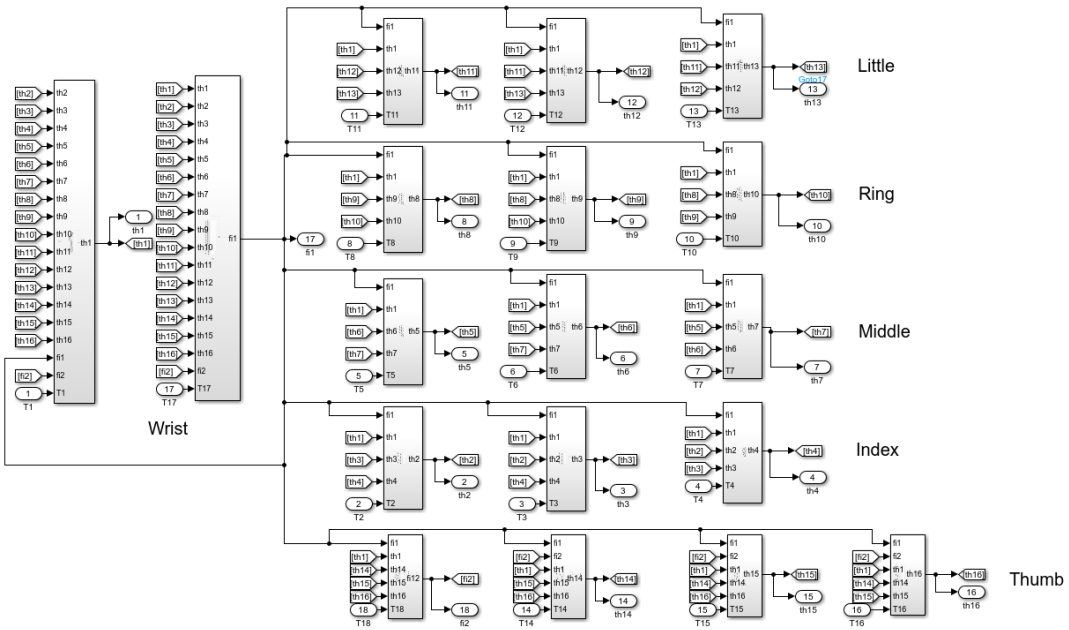

Figure 3. Step 1 in Simulink Model

The second step, **Step 2** block defines the variables that are the output of the system namely the actual angles of the system. In this step,

$$\theta_i = \theta_{ip}, \dot{\theta}_i = \dot{\theta}_{ip}, \ddot{\theta}_i = \ddot{\theta}_{ip} \; i = 1:18$$

are defined.

In the **Step 3**, each phalanx angle error $e_{\theta i}$ fi is determined,

$$e_{\theta i} = \theta_{id} - \theta_{ip}, \dot{e}_{\theta i} = \dot{\theta}_{id} - \dot{\theta}_{ip}, \ddot{e}_{\theta i} = \ddot{\theta}_{id} - \ddot{\theta}_{ip}, i = 1:18$$
$$\ddot{e}_{\theta i} = \ddot{\theta}_{id} - \ddot{\theta}_{ip}, \ddot{e}_{\theta i} = -\ddot{\theta}_{ip} + \ddot{\theta}_{id} \quad (15)$$

Where d is the desired position and p is the current position.

In the **step 4**, errors are updated.

$$e_{ia} = e_{\theta i} \rightarrow \dot{e}_{ia} = \dot{e}_{\theta i} \rightarrow \ddot{e}_{ia} = \ddot{e}_{\theta i} \rightarrow i = 1:18 \quad (16)$$

In block **step 5**, the SMC parameter $\xi_i = e_{ai}$ is defined.

$$\xi_i = e_{ai} \rightarrow \dot{\xi}_i = \dot{e}_{ai} \rightarrow i = 1:18 \quad (17)$$

The **Step 6** block creates 18 auxiliary sliding planes for HSMC. These sliding planes,

$$S_{ai} = C_i \xi_i + \dot{\xi}_i \rightarrow i = 1:18 \quad (18)$$

This is shown in Figure 2. They $C(C > 0)$ are positive coefficients. A new control variable is assigned. Auxiliary sliding planes are assigned as variables to the main sliding planes.

$$S_{mi} = S_{ai} \rightarrow i = 1:18 \quad (19)$$

For stability analysis, the Lyapunov function is checked at this stage.

$$\dot{S}_m \leq 0 \quad (20)$$

This stage refers to the steady state. At this stage, the tanh function is preferred to the signum function.

$$V_i = -k_{1\_i} S_{mi} - k_{2\_i} \tanh(S_{mi}) \rightarrow i = 1:18 \quad (21)$$

Where V is the variable, S_m is the main sliding plane and $k(k > 0)$ values are positive coefficients. When HPID is used at this stage, 18 auxiliary ITEA error-based data are generated. It is used for optimization operations. The same procedure is used for the PID controller,

$$V_i = (\theta_{id} - \zeta_i) * PID_i \rightarrow i = 1:18 \quad (22)$$

is defined as.

Therefore, the HSMC and HPID control systems are designed for the main system. A new control variable is defined in block **step 7**.

$$\ddot{e}_{ai} = V_i \rightarrow i = 1:18$$
$$V_{mi} = V_i - \ddot{\theta}_{id} \rightarrow i = 1:18 \quad (23)$$

is defined.

In **step 8** block, a new control variable is defined. This variable is assigned to the variable Uip. Here, the B values are abbreviations of all the constant and variable numbers in the denominator of the acceleration equation.

$$\begin{aligned} V_{mi} &= \ddot{\theta}_{ip} \rightarrow i = 1:16 \\ V_{mi} &= \ddot{\varphi}_{ip} \rightarrow i = 1:2 \\ U_{ip} &= V_{mi} * B_i \rightarrow i = 1:18 \end{aligned} \quad (24)$$

is defined as. A new control variable U is also defined in the ninth block. This **step 9**,

$$U_i = U_{ip} - G_i \rightarrow i = 1:18 \quad (25)$$

is defined as.

The G values here include all constant and variable numbers except the torque (τ) value in the numerator of the acceleration equation.

Step 10 block is the last step of the system. In this section a new control variable is defined. This step,

$$\tau_i = U_i \rightarrow i = 1:18 \quad (26)$$

is defined as. With this transformation, torque is input to the first step with the basic mathematical equations. These forces are limited to ± 30 N saturation. This limit range is taken as the average reference for axis motion[75].

The operations are initialized according to the trajectory control performance criterion used in control systems. The ITEA error was used as the performance criterion for the optimization process.

2.3.Optimization Algorithm

Particle Swarm Optimization (PSO) and Differential Evolution Optimization (DEO), which are metaheuristic algorithms, were used to tune the variable parameters of the controllers developed for the hand-wrist. The cost equation of optimization is *Vi* in Step 6.

2.3.1. Particle Swarm Optimization (PSO) Algorithm

The PSO algorithm is a population-based method for nonlinear functions. This nonlinear optimization algorithm based on particle swarms was inspired by social behaviour in nature [76]. The flowchart of this algorithm is shown in Algorithm 1.

The PSO algorithm starts by randomly distributing a population of n particles in the search space, inspired by nature. The particles move forward by comparing their data with the future particle based on their past behaviour. In this way, the past behaviours of the swarm and the particles are compared. It moves through an n-dimensional ecosystem at a dynamically adjusted learning rate. During this process, each particle stores its best value as P_best. The solution of a particle in the algorithm is the current value of the objective function depending on its position in the space system. All particles in the algorithm move forward to find the correct or closest solution in this objective function.

The search space is assumed to be D-dimensional and the D-dimensional vector with particle i is represented by $X_i = X_{i1}, X_{i2}..X_{iD}$. Let the velocity of this particle be represented by another D-dimensional vector $V_i = V_{i1}, V_{i2}..V_{iD}$. The best result of particle *i* so far is denoted by P_best in the same space. If G_{best}

is defined as the index of the best particle in the swarm, the velocity of particle i in dimension d is the moment component of the additional coefficient v_{id} from the previous iteration. c_1 and c_2 are the acceleration coefficients, which are the cognitive and social learning coefficients,

The search space is assumed to be D-dimensional and represents a D-dimensional vector with i particles. Let the velocity of this particle be represented by another D-dimensional vector. Let the best result of particle i so far be denoted by P_best in the same space. defined as the index of the best particle in the swarm, the velocity of particle i in dimension d is the instantaneous component of the addition coefficient v_id in the previous iteration. c is the acceleration coefficient, which is the cognitive and social learning coefficient. The equation for the velocity of particle i,

$$V_{id} = WV_{id}(t-1) + c_1 r_1 (P_{en\_iyi_{id}} - X_{id}(t-1)) + c_2 r_2 (G_{en\_iyi_{id}} - X_{id}(t-1)) \quad 27$$

is defined as. In this context, "W" is denoted as the coefficient of inertia, a fundamental parameter that governs the degree of repetition in the velocity of the particles. The coefficients "r_1" and "r_2" which are probabilistic values, are assigned random numbers within the interval of 0 to 1. The new position of the particles is determined by the following equation:

$$x_{id}(t) = x_{id}(t-1) + v(t) \quad 28$$

In the position equation, $x_{id}(t-1)$ is the current position of the particle. $v_{id}(t)$ is the update rate, and x_{id} is the new position. The value of the objective function used in the algorithm provides an improvement over the previous state until it converges to the local optimum.

Algorithm 1. PSO algorithm

Step 1.	Identify the parameters to be optimized and their limits
Step 2.	Initial positions of all particles are randomly assigned
Step 3.	Fitness values are obtained for optimization
Step 4.	By calculating the fitness values, the best values of the particles (P best) and the best value of the swarm (G best) are calculated
Step 5.	The fitness values of the particles are compared to the current best value P best . If the particle's value is better than the P best value, the current value is set as the new local best value.
Step 6.	The local best position values are compared with the global best position value. If the local best value is better, it is assigned as the global best location value.
Step 7.	The new velocity and position of the particles are redetermined
Step 8.	The termination condition is checked. If the criterion is met, the algorithm is terminated. Otherwise, the algorithm continues processing by recalculating the compliance values.
Step 9.	The best location G best is taken as the best optimal solution.

2.3.2. Differential Evolution (DE) Algorithm

The differential evolution algorithm is a heuristic designed to optimize nonlinear problems [77]. The problem-solving method of the DE algorithm is a population-based algorithm like the genetic algorithm. The flow diagram is given in Algorithm 2. The population size (PS), scaling factor (F) and crossover rate (CR) used in the algorithm flow parameters are taken as initial input values. The mutation or crossover process is of great importance for the optimization of the parameters. Mutation is to make random changes to the genes of the chromosome through progression. The crossover process moves the solution point forward. Thus, it offers more solutions.

The differential evolution algorithm runs until it reaches the maximum number of generations (G). When it reaches the maximum, the algorithm stops. In addition, the running of the algorithm can be determined not by the maximum number of generations, but by a stopping criterion. In this case, the algorithm will stop when the difference between the best and worst individuals decreases by the specified amount.

Algorithm 2. DEO algorithm

Step 1. For solution i from 1 to PS do
Step 2. Initialize the state Xi, G=0 of solution i.
Step 3. Evaluate the fitness value of solutions
Step 4. While the termination condition is not satisfied, do
Step 5. For each solution i from 1 to PS do
Step 6. Employ the mutation operator to generate the vector $V_{i,G}$ by Equation.
Step 7. Use the crossover operator to generate the trial vector $U_{i,G}$ by Equation
Step 8. ***If*** $f(U_{i,G}) < f(X_{i,G})$ ***then***
Step 9. Set $f(U_{i,G}) = f(X_{i,G+1})$
Step 10. Else
Step 11. $f(X_{i,G+1}) = f(U_{i,G})$
Step 12. End if
Step 13. End for
Step 14. End while

2.4.Simulation of the system

The system is simulated for passive exercise under disturbance. Passive exercises are performed without active muscle contraction, meaning you do not exert any effort with the limb being exercised or moved. So during the passive exercise simulation, the test setup does not apply any force to the fingers. The thumb and the other four fingers are performing flexion / extension movements. They are all restricted to the maximum angles of joints shown in Table 2 which are the natural limits of an average human hand. All initial actual angles are set to zero. The simulations are carried out in the order of HSMC-PSO, HSMC-DE, HPID-PSO and HPID-DE. ODE1 BE numerical solution algorithm is used with a step size of 0.1 Newton Euler 1 repetition solution selection. The ODE1 BE differential equations are solved according to the initial conditions in Table 3. The system runs with the torque input in the Step 1. In the simulation, 0.1sin (0.01t) disturbance input was used for each joint.

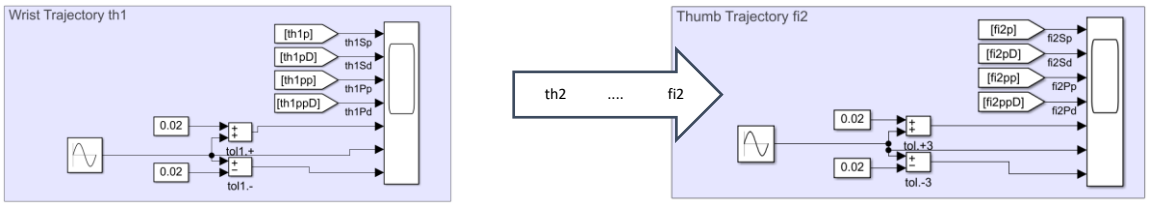

Figure 4. Reference trajectory to the scope

Table 2. Trajectory tracking parameters of the hand wrist system

Hand and Fingers		Angle	Flex. (rd.)	Ext. (rd.)	Trajectory tracking Sine (rad.)		
					Amplitude	Error	Frequency
Wrist	Fle/Ext	θ_{1d}	1.05	-1.05	1.050	---	
	Radyal/ Ulnar	φ_{1d}	0.43	-0.43	0.430	---	
Index	MCP	θ_{2d}	1.57	-0.70	1.135	0.435	
	PIP	θ_{3d}	1.92	0.00	0.960	0.960	
	DIP	θ_{4d}	1.48	-0.09	0.785	0.695	
Middle	MCP	θ_{5d}	1.57	-0.70	1.135	0.435	
	PIP	θ_{6d}	1.92	0.00	0.960	0.960	
	DIP	θ_{7d}	1.48	-0.09	0.785	0.695	
Ring	MCP	θ_{8d}	1.57	-0.70	1.135	0.435	XY :0.10
	PIP	θ_{9d}	2.09	0.00	1.045	1.045	XYZ:0.25
	DIP	θ_{10d}	1.48	-0.09	0.785	0.695	
Little	MCP	θ_{11d}	1.57	-0.70	1.135	0.435	
	PIP	θ_{12d}	2.36	0.00	1.180	1.180	
	DIP	θ_{13d}	1.48	-0.09	0.785	0.695	
Thumb	TMC	θ_{14d}	1.22	-0.26	0.740	0.480	
	MCP	θ_{15d}	1.40	0.00	0.700	0.700	
	IP	θ_{16d}	1.40	-0.17	0.785	0.615	
		φ_{2d}	0.34	-0.34	0.340	---	

Table 3. Initial conditions of the 18 DOF system

	Positions (rad)		
Wrist	$\varphi_1 = 0, \varphi_1 = 0.17$	$\theta_1 = 0, \dot{\theta}_1 = 0.17$	
Index	$\theta_2 = 0, \dot{\theta}_2 = 0.34$	$\theta_3 = 0, \dot{\theta}_3 = 0.52$	$\theta_4 = 0, \dot{\theta}_4 = 0.69$
Middle	$\theta_5 = 0, \dot{\theta}_5 = 0.34$	$\theta_6 = 0, \dot{\theta}_6 = 0.52$	$\theta_7 = 0, \dot{\theta}_7 = 0.69$
Ring	$\theta_8 = 0, \dot{\theta}_8 = 0.34$	$\theta_9 = 0, \dot{\theta}_9 = 1.20$	$\theta_{10} = 0, \dot{\theta}_{10} = 0.80$
Little	$\theta_{11} = 0, \dot{\theta}_{11} = 0.34$	$\theta_{12} = 0, \dot{\theta}_{12} = 0.52$	$\theta_{13} = 0, \dot{\theta}_{13} = 0.20$
Thumb	$\theta_{14} = 0, \dot{\theta}_{14} = 0.55$	$\theta_{15} = 0, \dot{\theta}_{15} = 0.65$	$\theta_{16} = 0, \dot{\theta}_{16} = 0.20$
	$\varphi_2 = 0, \dot{\varphi}_2 = 0.10$		

The link parameters used for the model are given in Table 4 and the controller parameters are given in Table 5. Surface friction is ignored. The search space of the system is given in Table 6. The HSMC optimization parameters are given in

Table **7**. The HPID optimization parameters are given in Table 8.

Table 4. Mean values of long finger phalanges lengths and weigh properties [25]

	m (kg)			L (m)		
Wrist	m1=0.222			L1=0.0482	La=0.0177	
Index	m2=0.030	m3=0.014	m4=0.007	L2=0.0198	L3=0.0111	L4=0.0079
Middle	m5=0.033	m6=0.016	m7=0.007	L5=0.0223	L6=0.0131	L7=0.0087
Ring	m8=0.022	m9=0.015	m10=0.007	L8=0.0206	L9=0.0128	L10=0.0086
Little	m11=0.018	m12=0.007	m13=0.004	L11=0.0163	L12=0.0090	L13=0.0079
Thumb	m14=0.033	m15=0.016	m16=0.01	L14=0.0231	L15=0.0157	L16=0.0108

Table 5. 18 DOF Model parameters

Cost Function		$\sum_{i=1}^{18}$ **ITAE**		Population	20	
Iteration		15		Time elapsed	0.2 (s)	
Cost	HSMC- PSO	**9111.206**	Convergence Time	HSMC- PSO	**776.472**	
	HSMC-DE	9112.914		HSMC-DE	1210.284	
	HPID-PSO	39469833.628		HPID-PSO	738.348	
	HPID-DE	**39469761.898**		HPID-DE	**687.446**	

Table 6. Algorithm search space for the 18 DOF system

HSMC - [C_i ξ_i $\dot{\xi}_i$]			**HPID - [P_i I_i D_i] i :18**		
Variable	Search Value		Variable	Search Value	
$C_1, \xi_{1\_1}, \dot{\xi}_{2\_1}$	[20 150 350]	± 0.5	P_1, I_1, D_1	[-100 -1 100]	± 0.5
$C_2, \xi_{1\_2}, \dot{\xi}_{2\_2}$	[50 100 300]	± 0.5	P_2, I_2, D_2	[-100 -1 100]	± 0.5
$C_3, \xi_{1\_3}, \dot{\xi}_{2\_3}$	[20 300 250]	± 0.5	P_3, I_3, D_3	[-100 -1 100]	± 0.5
$C_4, \xi_{1\_4}, \dot{\xi}_{2\_4}$	[20 200 250]	± 0.5	P_4, I_4, D_4	[-100 -1 100]	± 0.5
$C_5, \xi_{1\_5}, \dot{\xi}_{2\_5}$	[300 251 250]	± 0.5	P_5, I_5, D_5	[-100 -1 100]	± 0.5
$C_6, \xi_{1\_6}, \dot{\xi}_{2\_6}$	[50 115 150]	± 0.5	P_6, I_6, D_6	[-100 -1 100]	± 0.5
$C_7, \xi_{1\_7}, \dot{\xi}_{2\_7}$	[2 20 2]	± 0.5	P_7, I_7, D_7	[-100 -1 100]	± 0.5
$C_8, \xi_{1\_8}, \dot{\xi}_{2\_8}$	[2 20 2]	± 0.5	P_8, I_8, D_8	[-100 -1 100]	± 0.5
$C_9, \xi_{1\_9}, \dot{\xi}_{2\_9}$	[500 800 800]	± 0.5	P_9, I_9, D_9	[1e5 1e5 1e5]	± 0.5
$C_{10}, \xi_{1\_10}, \dot{\xi}_{2\_10}$	[300 400 100]	± 0.5	P_9, I_9, D_9	[1e5 1e5 1e5]	± 0.5
$C_{11}, \xi_{1\_11}, \dot{\xi}_{2\_11}$	[300 300 250]	± 0.5	P_{11}, I_{11}, D_{11}	[-800 -1 800]	± 0.5
$C_{12}, \xi_{1\_12}, \dot{\xi}_{2\_12}$	[1 250 400]	± 0.5	P_{12}, I_{12}, D_{12}	[-800 -1 800]	± 0.5
$C_{13}, \xi_{1\_13}, \dot{\xi}_{2\_13}$	[400 250 400]	± 0.5	P_{13}, I_{13}, D_{13}	[-800 -1 800]	± 0.5
$C_{14}, \xi_{1\_14}, \dot{\xi}_{2\_14}$	[600 600 800]	± 0.5	P_{14}, I_{14}, D_{14}	[-800 -1 800]	± 0.5
$C_{15}, \xi_{1\_15}, \dot{\xi}_{2\_15}$	[600 600 800]	± 0.5	P_{15}, I_{15}, D_{15}	[-5e4 -5e4 -5e4]	± 0.5
$C_{16}, \xi_{1\_16}, \dot{\xi}_{2\_16}$	[900 900 900]	± 0.5	P_{16}, I_{16}, D_{16}	[-1800 -1 1200]	± 0.5
$C_{17}, \xi_{1\_17}, \dot{\xi}_{2\_17}$	[200 800 100]	± 0.5	P_{17}, I_{17}, D_{17}	[-8e3 -8e3 -8e3]	± 0.5
$C_{18}, \xi_{1\_18}, \dot{\xi}_{2\_18}$	[10 800 100]	± 0.5	P_{18}, I_{18}, D_{18}	[-100 -1 100]	± 0.5

Table 7. HSMC Optimization Parameters for 18 DOF System

Variable	Search space (i =1:54)					
	HSMC- PSO			HSMC-DE		
i =1:3	**19.50**	**19.50**	**350.50**	19.73	149.73	350.12
i =4:6	**49.50**	**100.21**	**299.52**	50.49	100.00	299.98
i =7:9	**19.50**	**299.50**	**249.50**	19.53	299.89	250.16
i =10:12	**19.73**	**200.50**	**249.99**	19.91	200.01	250.44
i =13:15	**299.50**	**250.50**	**249.50**	299.75	251.11	249.96
i =16:18	**50.19**	**115.50**	**149.87**	49.50	114.59	149.50
i =19:21	**2.50**	**19.54**	**1.58**	1.79	19.79	1.88
i =22:24	**2.29**	**19.50**	**1.50**	1.50	20.04	2.04
i =25:27	**499.99**	**799.96**	**800.04**	500.24	800.50	799.96
i =28:30	**300.50**	**399.50**	**100.38**	300.22	399.50	99.764
i =31:33	**300.50**	**299.67**	**249.88**	299.50	299.54	249.75
i =34:36	**1.50**	**250.50**	**399.68**	1.18	250.50	399.94
i =37:39	**399.50**	**249.50**	**400.50**	399.86	249.50	400.25
i =40:42	**600.08**	**600.50**	**799.53**	600.16	600.50	799.68
i =43:45	**600.50**	**599.50**	**799.52**	599.89	599.55	800.19
i =46:48	**899.50**	**899.50**	**900.50**	899.59	899.64	899.95
i =49:51	**199.50**	**799.50**	**99.50**	199.67	799.50	99.63
i =52:54	**9.50**	**799.50**	**100.50**	9.57	799.50	99.80

Table 8. HPID Optimization Parameters for 18 DOF System

Variable	Search space (i =1:54)					
	HPID- PSO			HPID-DE		
i =1:3	**-99.87**	**-1.22**	**100.06**	-99.74	-1.12	99.85
i =4:6	**-100.20**	**-1.07**	**99.71**	-100.13	-0.50	100.33
i =7:9	**-99.94**	**-1.33**	**100.12**	-100.50	-0.55	99.68
i =10:12	**-100.14**	**-1.16**	**100.21**	-99.89	-0.63	100.39
i =13:15	**-99.71**	**-0.92**	**100.28**	-99.95	-0.50	100.10
i =16:18	**-99.78**	**-0.90**	**100.14**	-99.94	-0.82	99.72
i =19:21	**-100.10**	**-0.72**	**99.70**	-100.43	-0.53	100.07
i =22:24	**-99.67**	**-1.13**	**100.09**	-100.00	-1.49	100.36
i =25:27	**99999.59**	**99999.83**	**100000.3**	99999.54	99999.51	99999.50
i =28:30	**-9000.26**	**-9000.06**	**-8999.52**	-9000.50	-9000.25	-9000.46
i =31:33	**-800.06**	**-1.40**	**799.97**	-799.99	-0.75	799.50
i =34:36	**-799.87**	**-0.86**	**799.82**	-799.98	-1.24	800.34
i =37:39	**-800.27**	**-0.97**	**800.11**	-799.50	-0.64	799.64
i =40:42	**-799.98**	**-1.38**	**799.97**	-800.19	-1.28	800.06
i =43:45	**-49999.89**	**-49999.69**	**-50000.19**	-49999.50	-49999.91	-50000.49
i =46:48	**-1799.68**	**-1.07**	**1199.93**	-1799.98	-1.27	1200.00
i =49:51	**-7999.79**	**-8000.47**	**-8000.09**	-7999.84	-7999.59	-8000.31
i =52:54	**-100.32**	**-0.67**	**99.89**	-99.72	-1.25	100.50

3. RESULTS AND DISCUSSION

The reference trajectory values were determined based on the average limits of a real human hand.

The reference values used for trajectory tracking in the wrist rehabilitation exercise are provided in Table 2. The allowable tolerance band is set as ± 0.02 in the figures as red and green. They are represented as zoomed on the left corners of the figures.

Wrist flexion-extension trajectory tracking, angular error, torque and sliding plane plots, and radial-ulnar plots are shown in Figure 5. In the plots, 'Sd' represents HSMC-DEO and 'Sp' represents HSMC-PSO. 'Pd' represents HPID-DG and 'Pp' represents HPID-PSO. The sections where the system's settling time occurs are shown in the zoomed-in window. In the wrist exercise, the PSO and DG algorithms are equivalent. However, in terms of settling time, PSO appears to be more successful. The details are provided in Table 9.

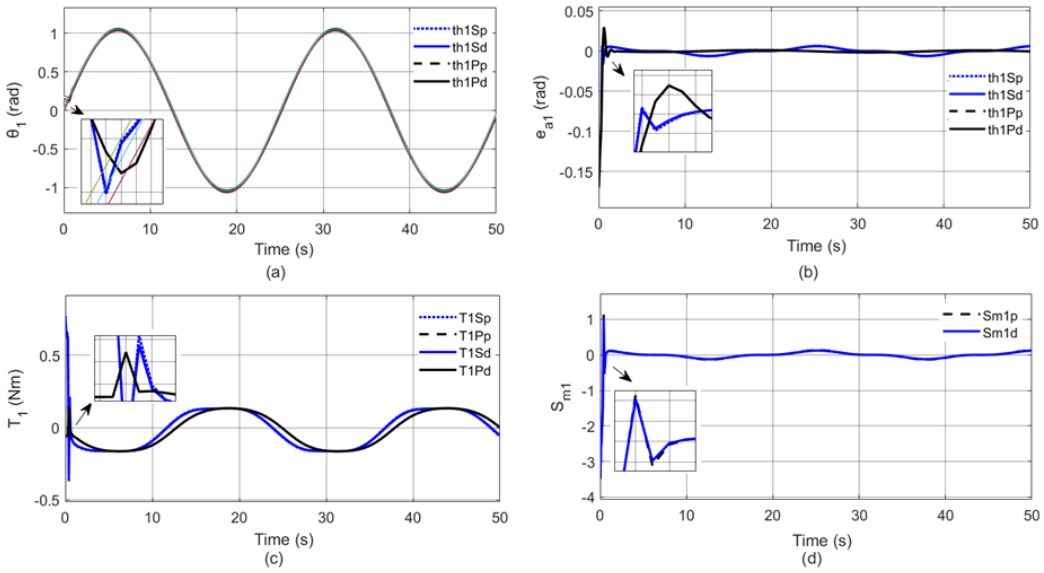

Figure 5. Wrist flexion-extension (a) Trajectory control, (b) Error (c) Torque (d) Sliding plane Sd: HSMC-DEO, Sp: HSMC-PSO, Pd: HPID-DG, Pp: HPID-PSO.

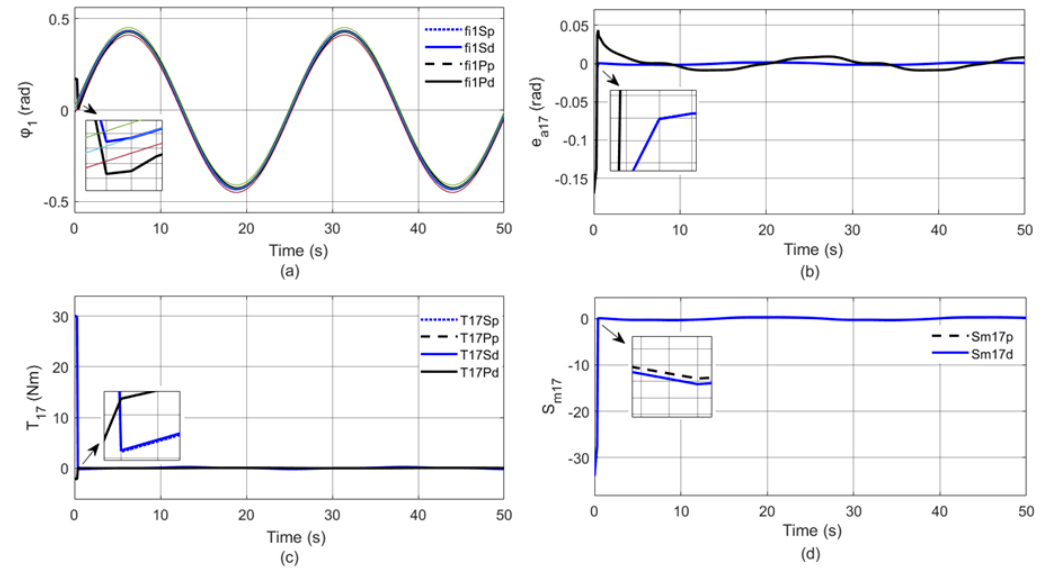

Figure 6. Radial/ulnar wrist perturbation (a) Trajectory control, (b) Error (c) Torque (d) Sliding plane Sd: HSMC-DEO, Sp: HSMC-PSO, Pd: HPID-DG, Pp: HPID-PSO.

The results for flexion-extension and radial-ulnar motion of the wrist are shown in Figure 6. Since the tracking performances of both controllers seem similar, HSMC is more stable than HPID. In terms of optimization algorithms, HSMC-PSO is faster, while the torque value of HSMC-DG is smaller.

Trajectory tracking, error, torque, and sliding plane plots for the MCP joint, PIP joint and DIP joint of the index finger are shown in Figure 7, Figure 8 , Figure 9, respectively.

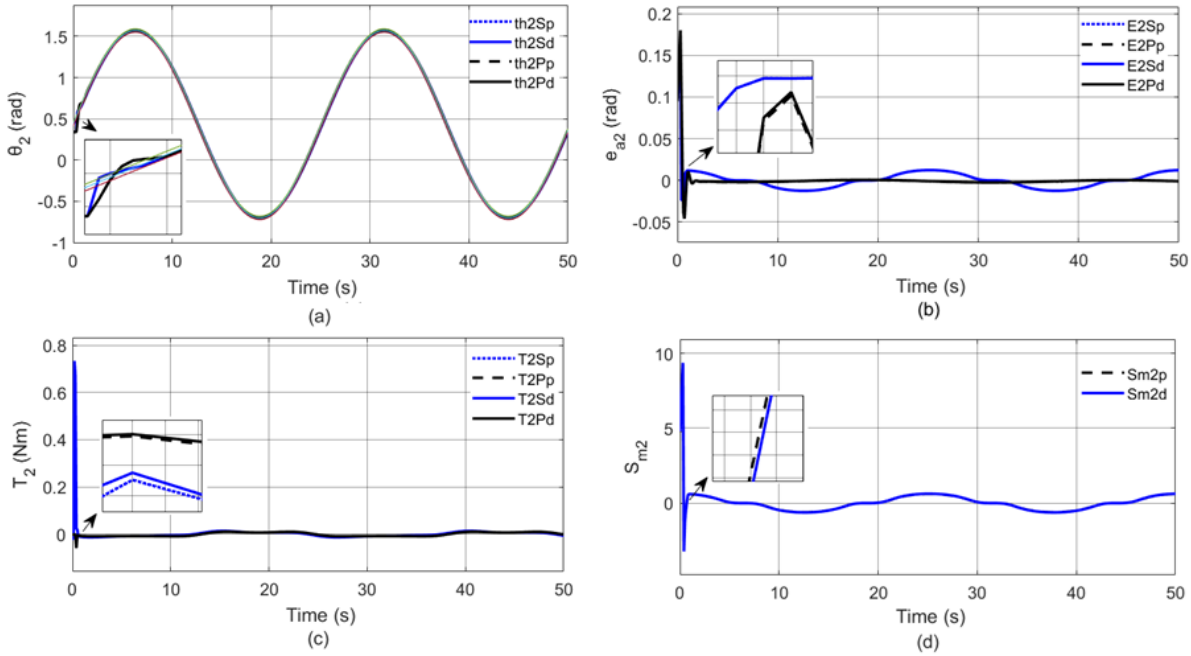

Figure 7. Index finger-MCP (a) Trajectory control, (b) Error (c) Torque (d) Sliding plane
Sd: HSMC-DEO, Sp: HSMC-PSO, Pd: HPID-DG, Pp: HPID-PSO

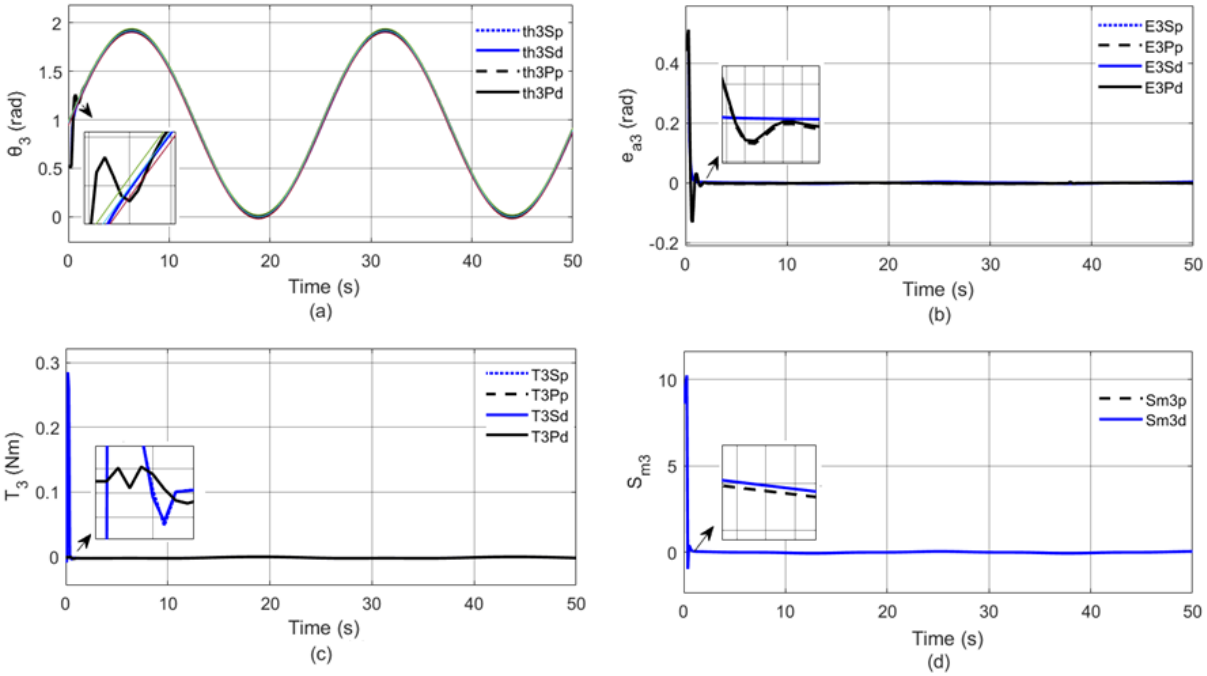

Figure 8. Index finger-PIP (a) Trajectory control, (b) Error (c) Torque (d) Sliding plane
Sd: HSMC-DEO, Sp: HSMC-PSO, Pd: HPID-DG, Pp: HPID-PSO

According to the results shown in Table 9, index finger trajectory tracking for MCP, PIP, and DIP joints are successful. Although the HSMC and HPID trajectory tracking performances are in tolerable band, the settling time for HPID is longer. In terms of optimization algorithms, it is seen that HSMC-PSO creates a smaller sliding plane. Trajectory tracking, error, torque, and sliding plane plots for the MCP joint, PIP joint and DIP joint of the middle finger are shown in Figure 10,Figure 11 and Figure 12, respectively.

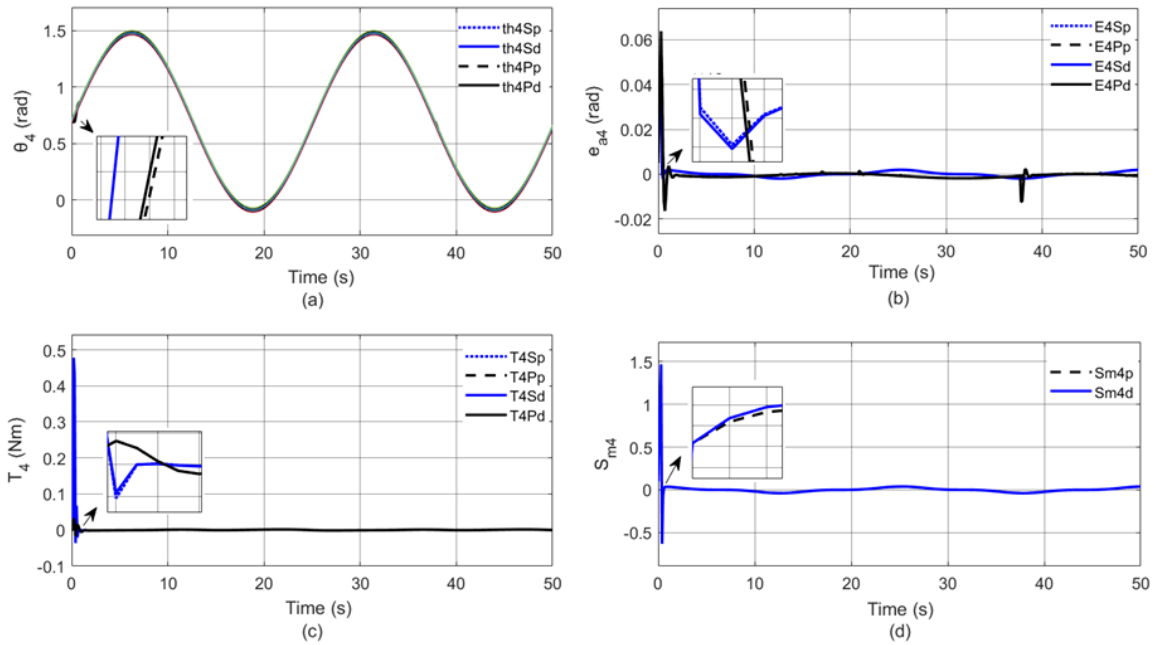

Figure 9. Index finger-DIP (a) Trajectory control, (b) Error (c) Torque (d) Sliding plane
Sd: HSMC-DEO, Sp: HSMC-PSO, Pd: HPID-DG, Pp: HPID-PSO

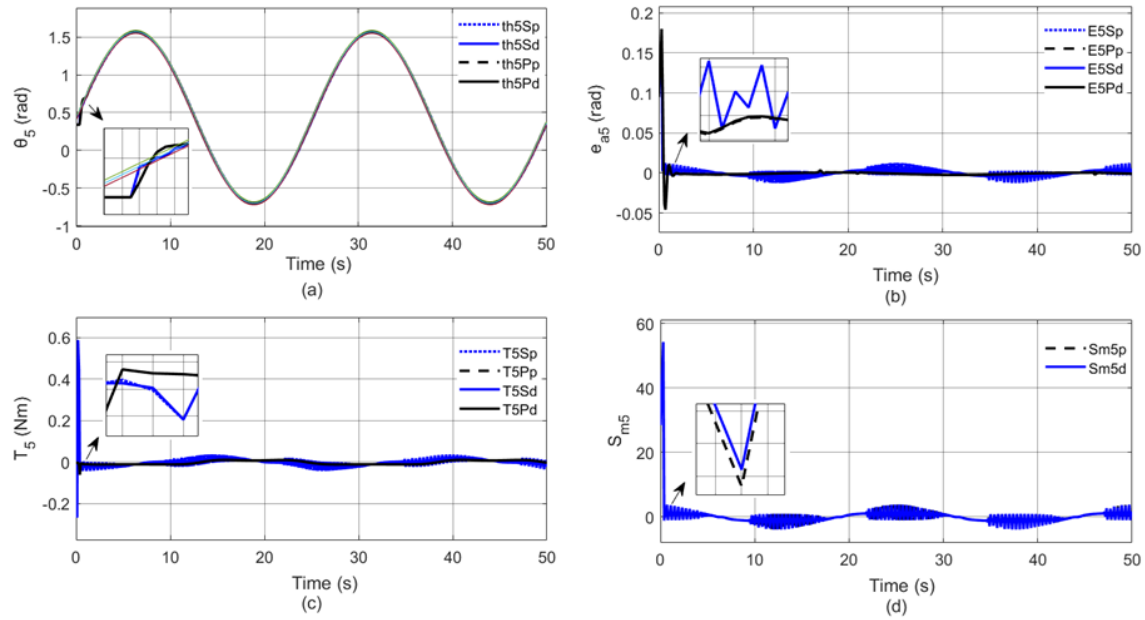

Figure 10. Middle finger-MCP (a) Trajectory control (b) Error (c) Torque (d) Sliding plane
Sd: HSMC-DEO, Sp: HSMC-PSO, Pd: HPID-DG, Pp: HPID-PSO

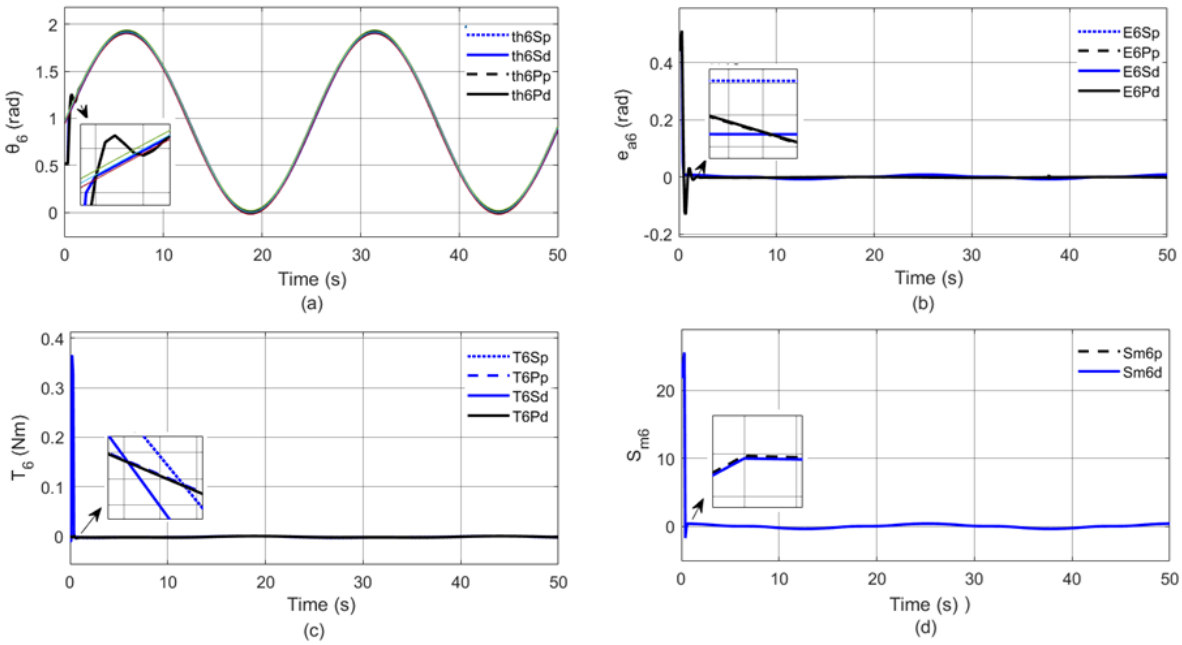

Figure 11. Middle finger -PIP (a) Trajectory control, (b) Error (c) Torque (d) Sliding plane
Sd: HSMC-DEO, Sp: HSMC-PSO, Pd: HPID-DG, Pp: HPID-PSO

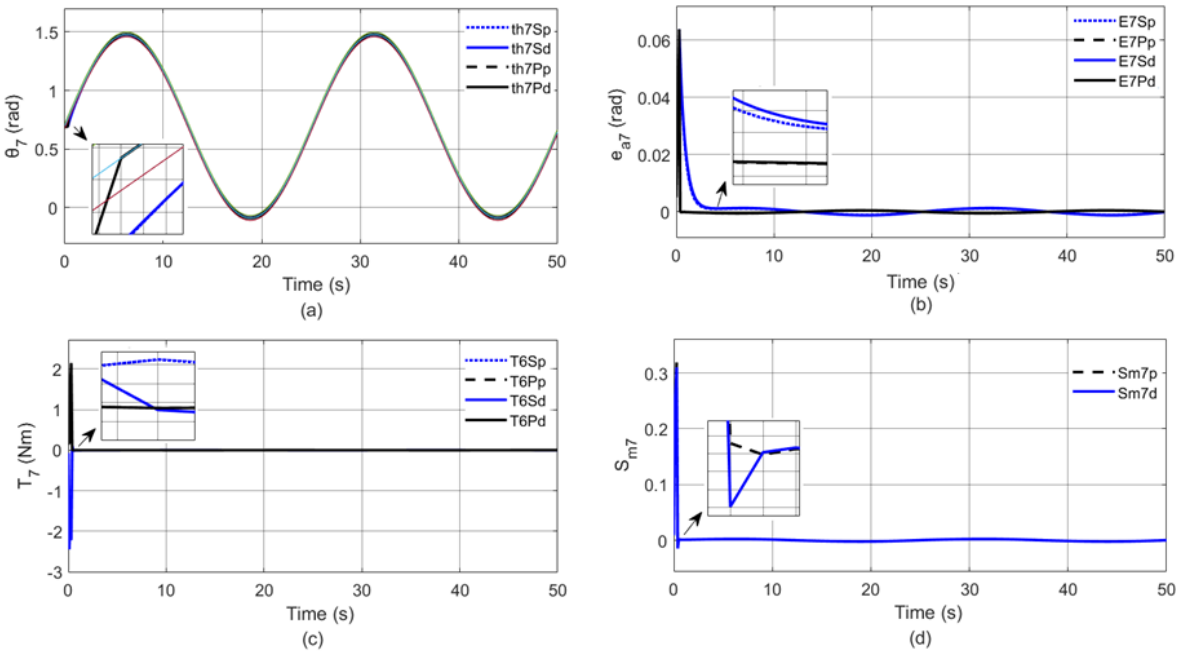

Figure 12. Middle finger -DIP (a) Trajectory control, (b) Error (c) Torque (d) Sliding plane
Sd: HSMC-DEO, Sp: HSMC-PSO, Pd: HPID-DG, Pp: HPID-PSO

According to the results shown in Table 9, the MCP, PIP, and DIP joints of the middle finger were found to be successful in trajectory tracking. It was observed that HSMC and HPID have good trajectory tracking, but HSMC torque values were higher. In terms of optimization algorithms, HPID-PSO and HPID-DE were found to be equivalent. Trajectory tracking, angular error, torque, and sliding plane plots for the MCP, PIP and DIP joints of the ring finger are shown in Figure 13, Figure 14 and Figure 15.

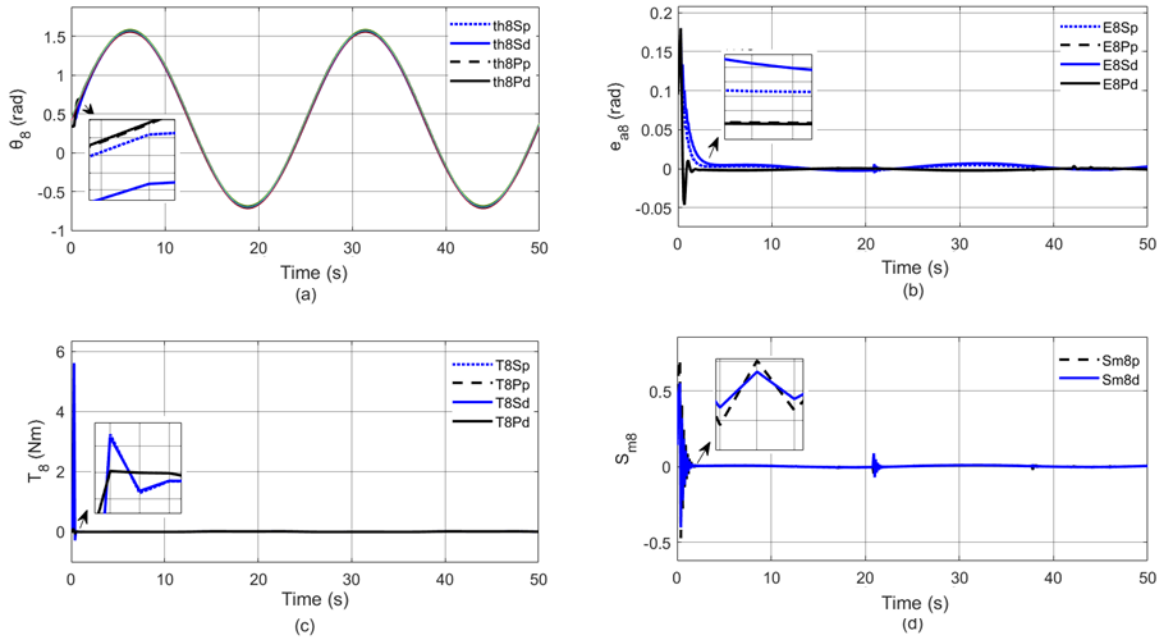

Figure 13. Ring finger- MCP (a) Trajectory control, (b) Error (c) Torque (d) Sliding plane
Sd: HSMC-DEO, Sp: HSMC-PSO, Pd: HPID-DG, Pp: HPID-PSO

According to the results shown in Table 9, it is observed that the MCP, PIP, and DIP joints of the ring finger are successful in trajectory tracking. HPID performed better trajectory tracking, but the torque values of HSMC were lower. In terms of optimization algorithms, it is seen that HPID-DE is more efficient.

Trajectory tracking, angular error, torque, and sliding plane plots for the MCP, PIP and DIP joints of the little finger are shown in Figure 16 , Figure 17 and Figure 18, respectively.

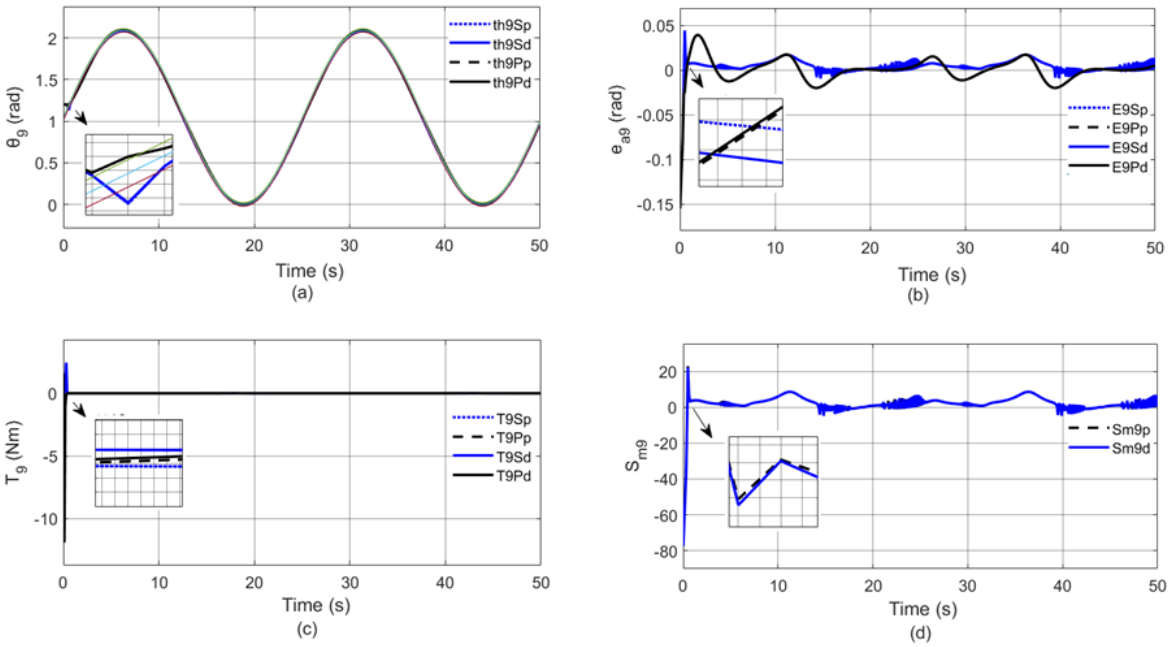

Figure 14. Ring finger- PIP (a) Trajectory control, (b) Error value, (c) Torque value, (d) Sliding plane
Sd: HSMC-DEO, Sp: HSMC-PSO, Pd: HPID-DG, Pp: HPID-PSO

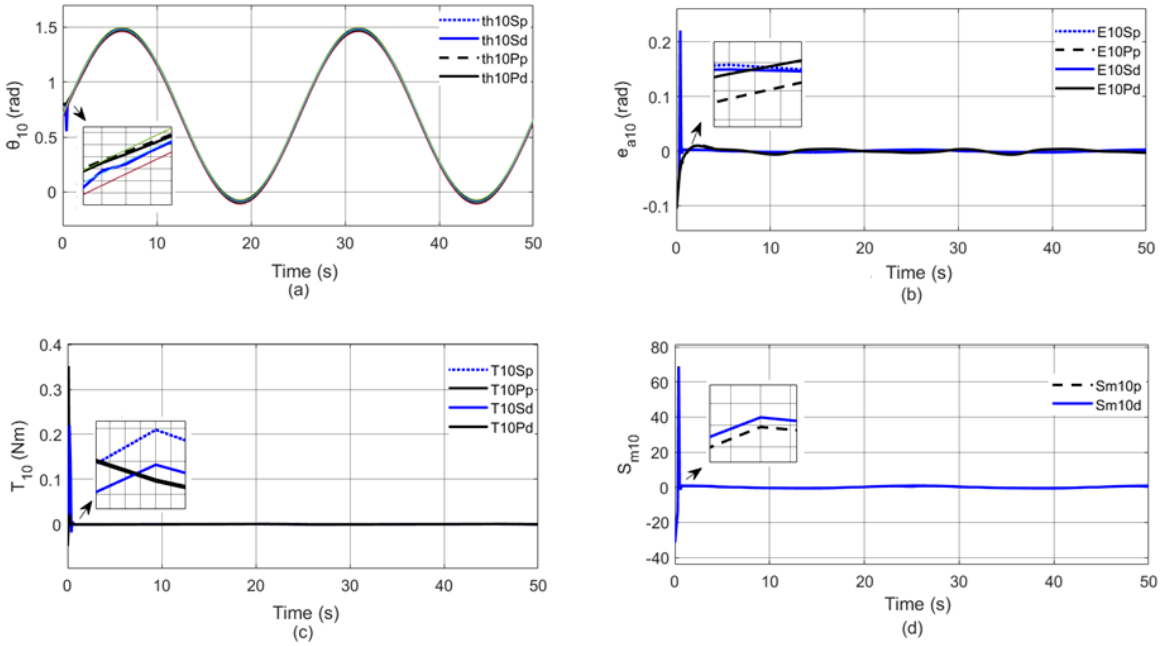

Figure 15. Ring finger- DIP (a) Trajectory control, (b) Error (c) Torque (d) Sliding plane
Sd: HSMC-DEO, Sp: HSMC-PSO, Pd: HPID-DG, Pp: HPID-PSO

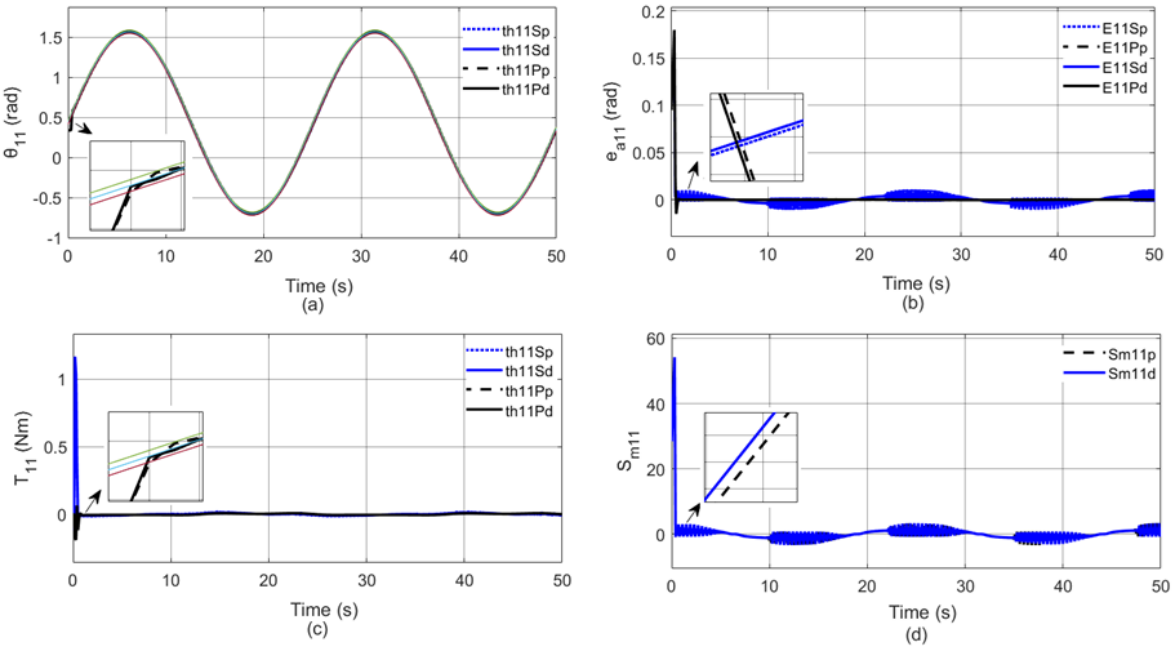

Figure 16. Little finger- MCP (a) Trajectory control, (b) Error (c) Torque (d) Sliding plane
Sd: HSMC-DEO, Sp: HSMC-PSO, Pd: HPID-DG, Pp: HPID-PSO

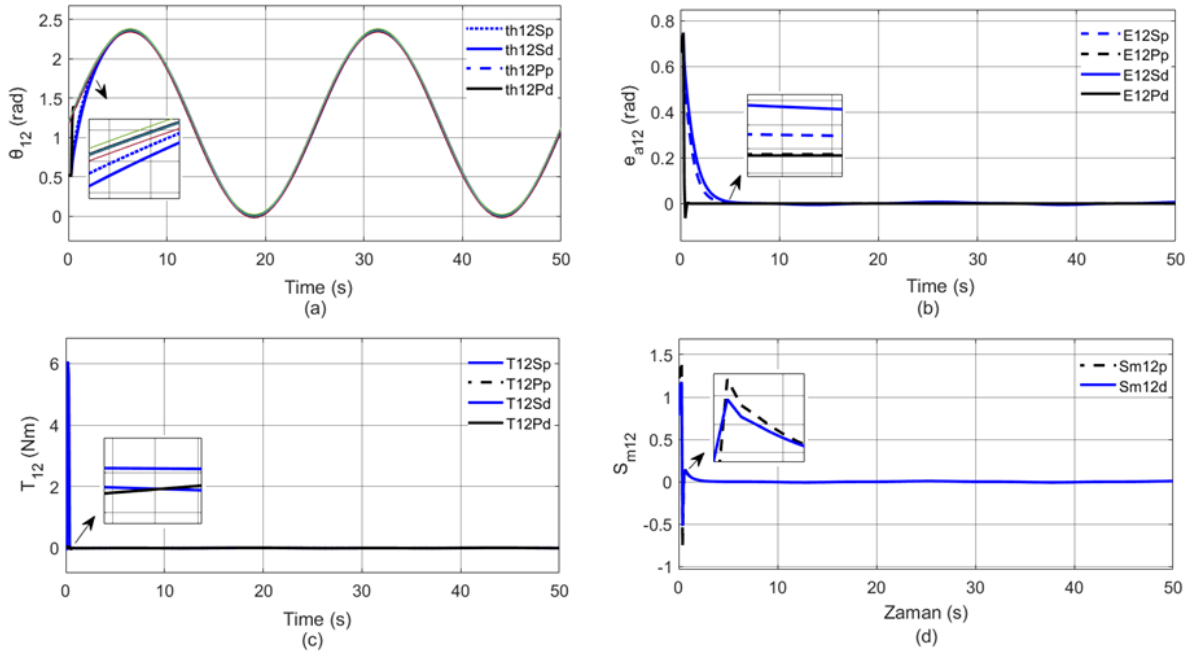

Figure 17. Little finger- PIP (a) Trajectory control, (b) Error (c) Torque (d) Sliding plane
Sd: HSMC-DEO, Sp: HSMC-PSO, Pd: HPID-DG, Pp: HPID-PSO

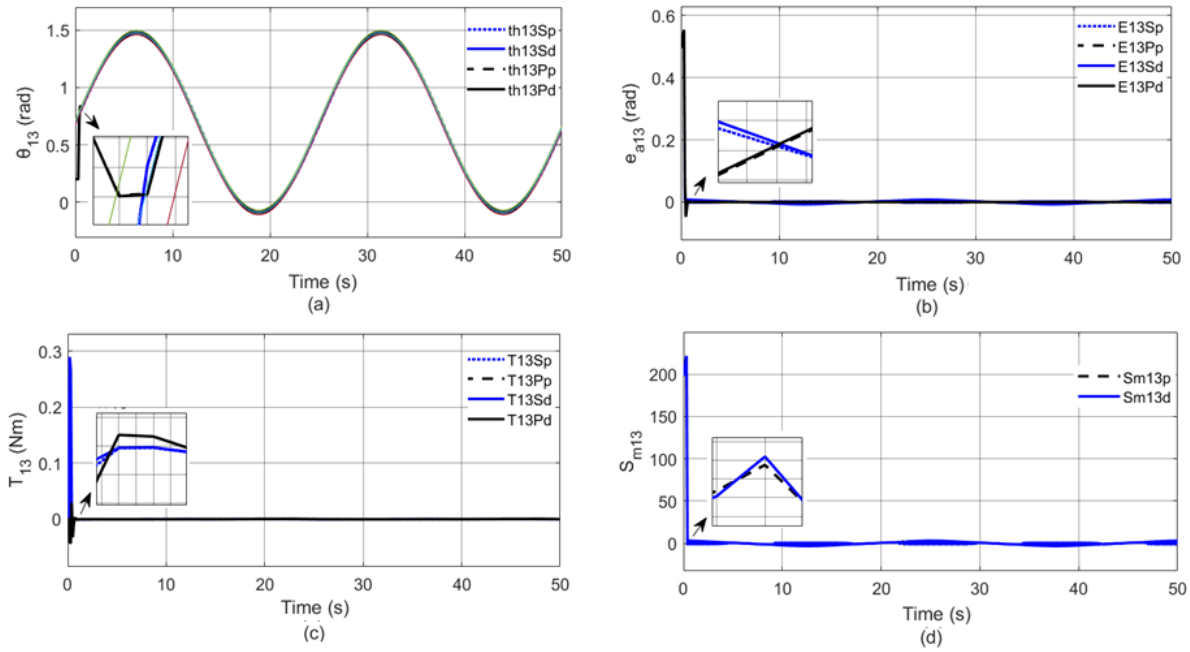

Figure 18. Little finger- DIP (a) Trajectory control, (b) Error (c) Torque (d) Sliding plane
Sd: HSMC-DEO, Sp: HSMC-PSO, Pd: HPID-DG, Pp: HPID-PSO

According to the results shown in Table 9, the MCP, PIP, and DIP joints of the little finger were found to be successful in trajectory tracking. The reference trajectory tracking was successful with both control methods. It was observed that HSMC and HPID performed accurate trajectory tracking, but the HPID torque values were lower. In terms of optimization algorithms, it is seen that HPID-PSO is more successful.

Trajectory tracking, angle error, torque, and sliding plane plots for the TMC joint, MCP joint, IP joint of the thumb are shown in Figure 19, Figure 20 and Figure 21, respectively. Abduction-adduction trajectory tracking, angle error, torque, and sliding plane plots for the thumb are shown in Figure 22.

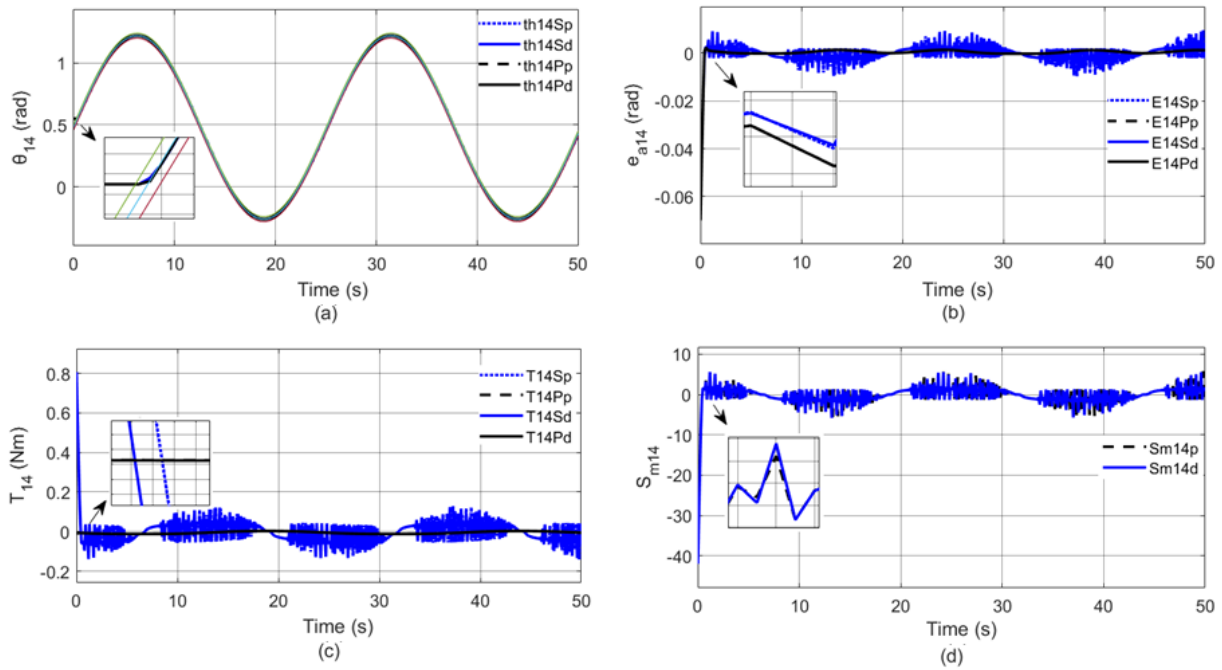

Figure 19. Thumb-TMC (a) Trajectory control, (b) Error value, (c) Torque value, (d) Sliding plane
Sd: HSMC-DEO, Sp: HSMC-PSO, Pd: HPID-DG, Pp: HPID-PSO

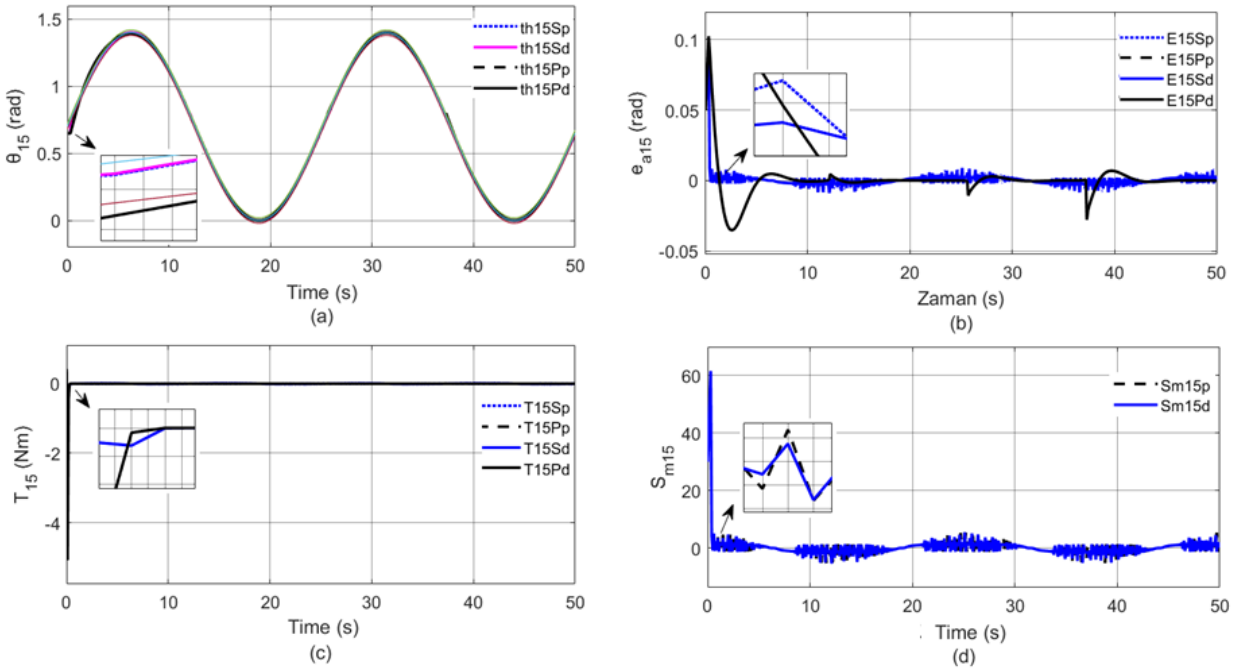

Figure 20. Thumb-MCP (a) Trajectory control, (b) Error (c) Torque (d) Sliding plane
Sd: HSMC-DEO, Sp: HSMC-PSO, Pd: HPID-DG, Pp: HPID-PSO

According to the results shown in Table 9, it was observed that TMC, MCP, and IP joints of the thumb during Abb-Add. were successful in trajectory tracking. Reference trajectory tracking was successful in both control methods. It was observed that HSMC and HPID performed accurate trajectory tracking in TMC, IP, and Ab-Ad joints, but HPID torque values were lower. In terms of optimization algorithms, it is seen that HPID-PSO is better.

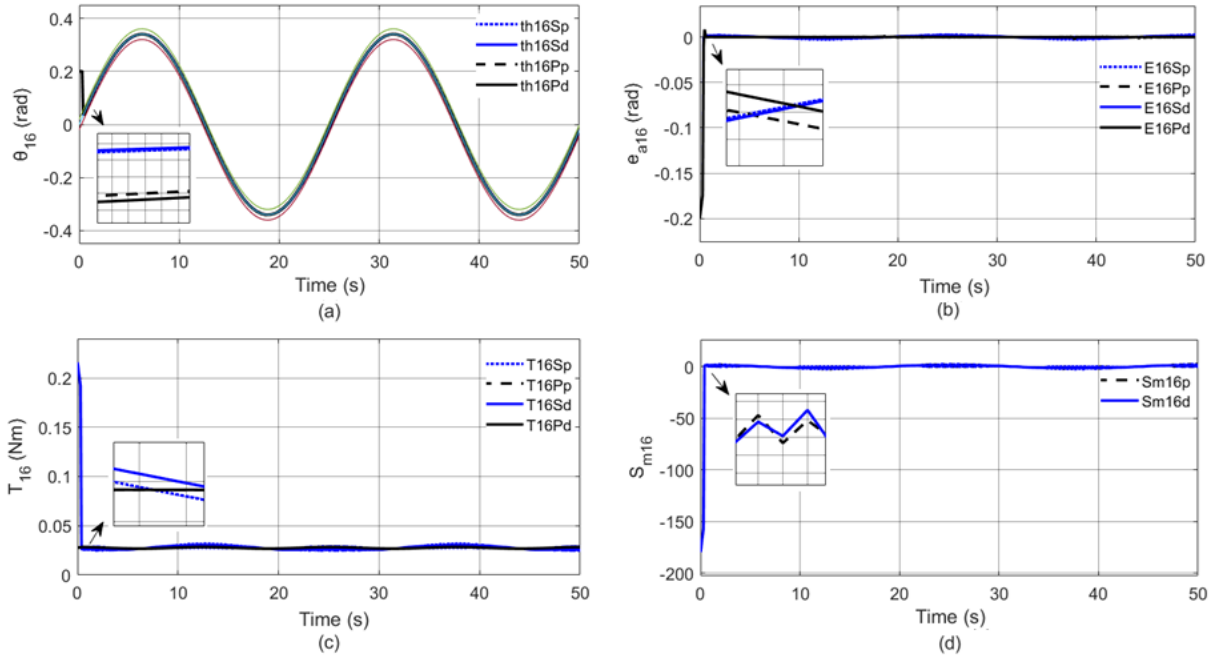

Figure 21. Thumb-IP (a) Trajectory control, (b) Error (c) Torque (d) Sliding plane
Sd: HSMC-DEO, Sp: HSMC-PSO, Pd: HPID-DG, Pp: HPID-PSO

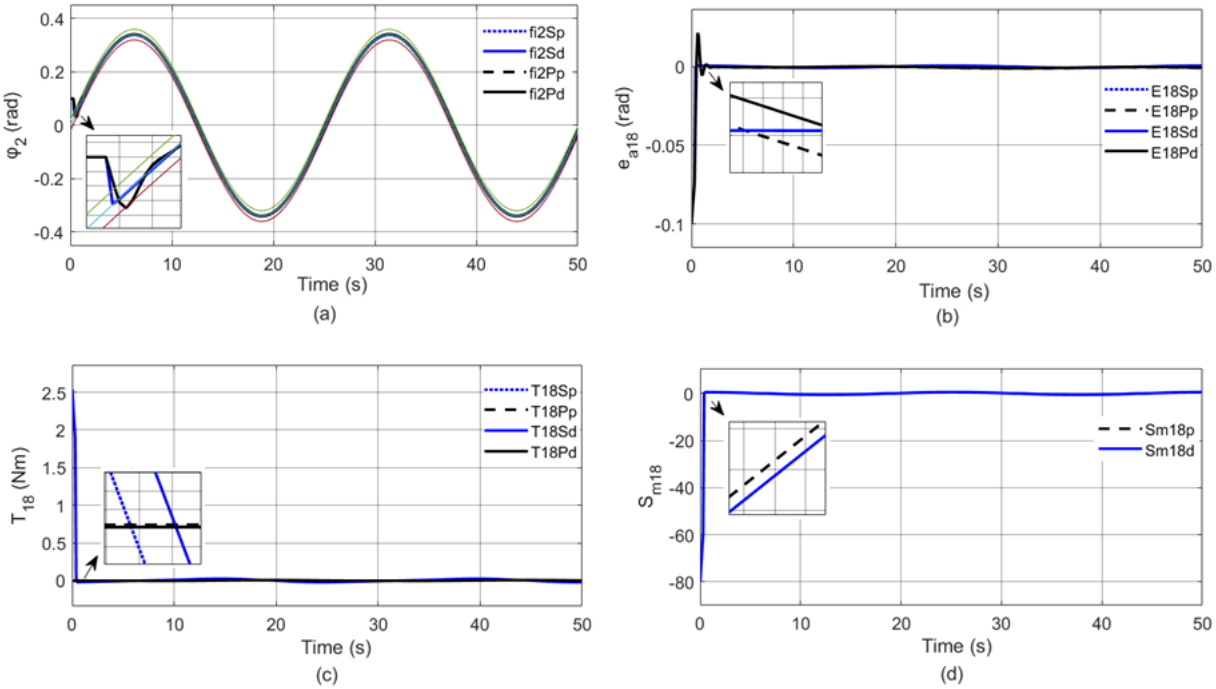

Figure 22. Thumb abduction-phalangeal (a) Trajectory control, (b) Error (c) Torque d) Sliding plane
Sd: HSMC-DEO, Sp: HSMC-PSO, Pd: HPID-DG, Pp: HPID-PSO

During the simulations, maximum overshoot, settling time, torque values, and sliding surface values for each finger are shown in Table 9. In general, it can be observed that the performances of HSMC and HPID are similar, only HSMC is faster.

Table 9. Simulation results (allowable tolerance 0.02)

		Cont. Type	Mp	ts	Torque (Nm)	(S_m) max.	
Wrist	Flex.-Ext.	HSMC- PSO	**non**	**0.3724**	-0.3699	S_{m1}	1.1295
		HSMC-DG	**non**	0.3746	-0.3460		**1.0402**
		HPID-PSO	0.0298	0.7226	**-0.1629**		
		HPID-DG	0.0298	0.7226	**-0.1629**		
	Rad-Uln.	HSMC- PSO	**non**	**0.3892**	30.0000	S_{m17}	**-33.9150**
		HSMC-DG	**non**	**0.3892**	30.0000		-33.9440
		HPID-PSO	0.0437	1.6537	-2.1850		
		HPID-DG	0.0437	1.6537	**-2.1849**		
Index	MCP	HSMC- PSO	**0.1800**	**0.5256**	0.7344	S_{m2}	**9.2457**
		HSMC-DG	**0.1800**	0.5286	0.7322		9.3751
		HPID-PSO	**0.1800**	0.8318	-0.0606		
		HPID-DG	**0.1800**	0.8307	**-0.0603**		
	PIP	HSMC- PSO	**0.5119**	0.6759	0.2851	S_{m3}	**10.2222**
		HSMC-DG	**0.5119**	**0.6753**	0.2844		10.2418
		HPID-PSO	**0.5119**	1.1674	-0.0028		
		HPID-DG	**0.5119**	1.1721	-0.0028		
	DIP	HSMC- PSO	**0.0638**	0.3694	0.4781	S_{m4}	**1.4424**
		HSMC-DG	**0.0638**	**0.3689**	0.4760		1.4669
		HPID-PSO	**0.0638**	0.4711	**0.0316**		
		HPID-DG	**0.0638**	0.4630	**0.0316**		
Middle	MCP	HSMC- PSO	**0.1800**	**0.3900**	0.5893	S_{m5}	**54.2065**
		HSMC-DG	**0.1800**	**0.3900**	0.5871		54.2520
		HPID-PSO	**0.1800**	0.8312	**-0.0614**		
		HPID-DG	**0.1800**	0.8326	**-0.0614**		
	PIP	HSMC- PSO	**0.5119**	0.4714	0.3661	S_{m6}	**25.5802**
		HSMC-DG	**0.5119**	**0.4709**	0.3652		**25.5802**
		HPID-PSO	**0.5119**	1.1722	-0.0037		
		HPID-DG	**0.5119**	1.1720	-0.0037		
	DIP	HSMC- PSO	**0.0638**	0.9678	-2.4425	S_{m7}	0.3195
		HSMC-DG	**0.0638**	1.0003	-2.4153		**0.3102**
		HPID-PSO	**0.0638**	**0.3685**	**2.1407**		
		HPID-DG	**0.0638**	0.3686	2.1468		
Ring	MCP	HSMC- PSO	**0.1800**	1.3706	5.6086	S_{m8}	0.7088
		HSMC-DG	**0.1800**	1.9527	5.6120		**0.5532**
		HPID-PSO	**0.1800**	0.8332	**0.0890**		
		HPID-DG	**0.1800**	**0.8331**	0.0996		
	PIP	HSMC- PSO	0.0443	0.5838	2.4479	S_{m9}	22.8665
		HSMC-DG	0.0429	0.5837	2.4487		22.1481
		HPID-PSO	0.0391	39.5001	-11.9104		
		HPID-DG	0.0391	39.5026	-11.9103		
	DIP	HSMC- PSO	0.2203	0.4961	0.2202	S_{m10}	68.8780
		HSMC-DG	0.2192	0.4962	**0.2197**		**68.4787**
		HPID-PSO	**non**	0.6250	0.3521		
		HPID-DG	**non**	**0.4878**	0.3521		
Little	MCP	HSMC- PSO	**0.1800**	**0.3903**	1.1668	S_{m11}	**54.2067**
		HSMC-DG	**0.1800**	**0.3903**	1.1668		**54.2067**
		HPID-PSO	**0.1800**	0.4086	**-0.1892**		
		HPID-DG	**0.1800**	0.4083	**-0.1892**		
	PIP	HSMC- PSO	**0.7484**	3.2025	6.0719	S_{m12}	1.4170
		HSMC-DG	**0.7484**	3.9065	6.0645		1.1788
		HPID-PSO	**0.7484**	**0.6169**	**-0.0543**		
		HPID-DG	**0.7484**	0.6172	-0.0545		
	DIP	HSMC- PSO	**0.5538**	0.3980	0.2879	S_{m13}	**221.4550**

		HSMC-DG	**0.5538**	**0.3979**	0.2874		221.6494
		HPID-PSO	**0.5538**	0.5934	**-0.0436**		
		HPID-DG	**0.5538**	0.5928	**-0.0436**		
Thumb	TMC	HSMC- PSO	**non**	**0.2704**	-0.1402	S_{m14}	5.6800
		HSMC-DG	**non**	**0.2704**	-0.1343		**5.5800**
		HPID-PSO	**non**	**0.2704**	**-0.0010**		
		HPID-DG	**non**	**0.2704**	**-0.0010**		
	MCP	HSMC- PSO	**0.1024**	**0.3874**	**-0.0623**	S_{m15}	**61.6240**
		HSMC-DG	**0.1024**	**0.3874**	**-0.0623**		61.6340
		HPID-PSO	**0.1024**	37.4505	-5.0779		
		HPID-DG	**0.1024**	37.4475	-5.0780		
	IP	HSMC- PSO	**non**	**0.3889**	0.0326	S_{m16}	3.3550
		HSMC-DG	**non**	**0.3889**	0.0328		**3.3040**
		HPID-PSO	**non**	0.3933	**0.0282**		
		HPID-DG	**non**	0.3933	**0.0282**		
	Ab- Ad.	HSMC- PSO	**non**	**0.3739**	-0.0199	S_{m18}	**-0.5300**
		HSMC-DG	**non**	**0.3739**	-0.0199		**-0.5300**
		HPID-PSO	0.0213	0.6560	**-0.0030**		
		HPID-DG	0.0215	0.6680	**-0.0030**		

4. CONCLUSIONS

In the field of hand and wrist rehabilitation robots, there are few studies in the literature for multi DOF systems. Most of the studies are focused on the development of systems with few degrees of freedom. Novel control methodologies Hierarchical Sliding Mode Control and Hierarchical PID control were used to control the proposed hand and wrist rehabilitation robot. According to the simulation of the 18-degrees-of-freedom system, successful results were achieved. HSMC showed superior performance than the HPID. Moreover, the use of optimization methods for controller parameters selection are searched. PSO algorithm gave faster and more robust results in the optimization processes with both HSMC and HPID. The findings demonstrate that HSMC effectively improve trajectory tracking, reducing mean absolute and normalized root mean square (NRMS) errors compared to HPID controllers. The proposed approach shows promising potential for real implementation, enhancing the efficiency of rehabilitation devices.

Declaration of Ethical Standards

The authors of this article declare that the materials and methods used in this study do not require ethical committee permission and/or legal-special permission.

Credit Authorship Contribution Statement

Author1: Methodology, Resources, Software Development, Analysis, Writing
Author2: Methodology, Conceptualization, Investigation, Writing -review & editing, Supervision

Declaration of Competing Interest

The authors of this article declare that they have no significant competing financial, professional, or personal interests that might have influenced the performance or presentation of the work described in this manuscript.

Funding / Acknowledgements

The research presented in this paper was supported by Karadeniz Technical University. The project

has been supported by the Scientific Research Projects Coordination Unit with the project ID 10664.

Data Availability

Data available on request from the author.

REFERENCES

[1] T. Wang, D. Mantini, and C. R. Gillebert, "The potential of real-time fMRI neurofeedback for stroke rehabilitation: A systematic review," (in eng), *Cortex,* vol. 107, pp. 148-165, Oct 2018.

[2] F. Molteni, G. Gasperini, G. Cannaviello, and E. Guanziroli, "Exoskeleton and End-Effector Robots for Upper and Lower Limbs Rehabilitation: Narrative Review," (in eng), *Pm r,* vol. 10, no. 9 Suppl 2, pp. S174-s188, Sep 2018.

[3] H. B. Hoffman and G. L. Blakey, "New design of dynamic orthoses for neurological conditions," (in eng), *NeuroRehabilitation,* vol. 28, no. 1, pp. 55-61, 2011.

[4] A. Rahman and A. Al-Jumaily, "Design and Development of a Bilateral Therapeutic Hand Device for Stroke Rehabilitation," vol. 10, no. 12, p. 405, 2013.

[5] C. N. Schabowsky, "Robot-Assisted Hand Movement Therapy after Stroke," Doctor of Philosophy, Department of Biomedical Engineering School of Engineering, The Catholic University of America, ProQuest LLC., 2010.

[6] U. Mayetin, "Taşınabilir Bilek Rehabilitasyon Robotu Tasarımı ve Geliştirilmesi," Ph.D, Biomedikal Mühendisliği, Kocaeli Üniversitesi, Fen Bilimleri Enstitüsü, 716593, 2022.

[7] J. Sumner, H. W. Lim, L. S. Chong, A. Bundele, A. Mukhopadhyay, and G. Kayambu, "Artificial intelligence in physical rehabilitation: A systematic review," *Artificial Intelligence in Medicine,* vol. 146, p. 102693, 2023/12/01/ 2023.

[8] A. C. McConnell *et al.*, "Robotic devices and brain-machine interfaces for hand rehabilitation post-stroke," (in eng), *J Rehabil Med,* vol. 49, no. 6, pp. 449-460, Jun 28 2017.

[9] T. Dickmann, N. J. Wilhelm, C. Glowalla, S. Haddadin, P. Van der Smagt, and R. Burgkart, "An Adaptive Mechatronic Exoskeleton for Force-Controlled Finger Rehabilitation," (in eng), *Front Robot AI,* vol. 8, p. 716451, 2021.

[10] Y. K. Ou, Y. L. Wang, H. C. Chang, and C. C. Chen, "Design and Development of a Wearable Exoskeleton System for Stroke Rehabilitation," (in eng), *Healthcare (Basel),* vol. 8, no. 1, Jan 15 2020.

[11] E. Pezent, "Design, Characterization, and Validation of the OpenWrist Exoskeleton," Master of Science Engineering, Mechanical Engineering, Rice University, Published by ProQuest LLC, 2017.

[12] C. N. Schabowsky, S. B. Godfrey, R. J. Holley, and P. S. Lum, "Development and pilot testing of HEXORR: hand EXOskeleton rehabilitation robot," (in eng), *J Neuroeng Rehabil,* vol. 7, p. 36, Jul 28 2010.

[13] N. Sun, G. Li, and L. Cheng, "Design and Validation of a Self-Aligning Index Finger Exoskeleton for Post-Stroke Rehabilitation," *IEEE Transactions on Neural Systems and Rehabilitation Engineering,* vol. 29, pp. 1513-1523, 2021.

[14] C. Liu, J. Lu, H. Yang, and K. Guo, "Current State of Robotics in Hand Rehabilitation after Stroke: A Systematic Review," *Applied Sciences*, vol. 12, no. 9. doi: 10.3390/app12094540

[15] J. Iqbal, N. G. Tsagarakis, and D. G. Caldwell, "Four-fingered lightweight exoskeleton robotic device accommodating different hand sizes," vol. 51, no. 12, pp. 888-890, 2015.

[16] D. Leonardis *et al.*, "An EMG-Controlled Robotic Hand Exoskeleton for Bilateral Rehabilitation," (in eng), *IEEE Trans Haptics,* vol. 8, no. 2, pp. 140-51, Apr-Jun 2015.

[17] R. Conti, E. Meli, and A. Ridolfi, "A novel kinematic architecture for portable hand exoskeletons," *Mechatronics,* vol. 35, pp. 192-207, 2016/05/01/ 2016.

[18] R. Conti *et al.*, "Kinematic synthesis and testing of a new portable hand exoskeleton," *Meccanica,* vol. 52, no. 11, pp. 2873-2897, 2017/09/01 2017.

[19] S. Kim, J. Lee, and J. Bae, "Analysis of Finger Muscular Forces using a Wearable Hand Exoskeleton

System," *Journal of Bionic Engineering,* vol. 14, no. 4, pp. 680-691, 2017/10/01/ 2017.

[20] S. Kim, J. Lee, W. Park, and J. Bae, "Quantitative evaluation of hand functions using a wearable hand exoskeleton system," (in eng), *IEEE Int Conf Rehabil Robot,* vol. 2017, pp. 1488-1493, Jul 2017.

[21] M. Decker and Y. J. I. W. H. C. Kim, "A hand exoskeleton device for robot assisted sensory-motor training after stroke," pp. 436-441, 2017.

[22] I. Jo, J. Lee, Y. Park, and J. Bae, "Design of a wearable hand exoskeleton for exercising flexion/extension of the fingers," (in eng), *IEEE Int Conf Rehabil Robot,* vol. 2017, pp. 1615-1620, Jul 2017.

[23] P. Sale, G. Sellin, M. Stefano, F. Becchi, and W. Sieklicki, "FEX a Fingers Extending eXoskeleton for Rehabilitation and Regaining Mobility," 2018.

[24] F. Zhang, L. Hua, Y. Fu, H. Chen, and S. Wang, "Design and development of a hand exoskeleton for rehabilitation of hand injuries," *Mechanism and Machine Theory,* vol. 73, pp. 103-116, 2014/03/01/ 2014.

[25] A. Lince *et al.*, "Design and testing of an under-actuated surface EMG-driven hand exoskeleton," (in eng), *IEEE Int Conf Rehabil Robot,* vol. 2017, pp. 670-675, Jul 2017.

[26] A. Bataller, J. A. Cabrera, M. Clavijo, and J. J. Castillo, "Evolutionary synthesis of mechanisms applied to the design of an exoskeleton for finger rehabilitation," *Mechanism and Machine Theory,* vol. 105, pp. 31-43, 2016/11/01/ 2016.

[27] I. Jo, Y. Park, J. Lee, and J. Bae, "A portable and spring-guided hand exoskeleton for exercising flexion/extension of the fingers," *Mechanism and Machine Theory,* vol. 135, pp. 176-191, 2019/05/01/ 2019.

[28] D. Marconi, A. Baldoni, Z. McKinney, M. Cempini, S. Crea, and N. Vitiello, "A novel hand exoskeleton with series elastic actuation for modulated torque transfer," *Mechatronics,* vol. 61, pp. 69-82, 2019/08/01/ 2019.

[29] M. Haghshenas-Jaryani, W. Carrigan, C. Nothnagle, and M. B. J. Wijesundara, "Sensorized soft robotic glove for continuous passive motion therapy," *EEE 6th. International Conference on Biomedical Robotics,* pp. 815-820, 2016.

[30] P. Polygerinos, Z. Wang, K. C. Galloway, R. J. Wood, C. J. J. R. Walsh, and A. Systems, "Soft robotic glove for combined assistance and at-home rehabilitation," vol. 73, pp. 135-143, 2015.

[31] H. K. Yap, B. W. K. Ang, J. H. Lim, J. C. H. Goh, C.-H. J. I. I. C. o. R. Yeow, and Automation, "A fabric-regulated soft robotic glove with user intent detection using EMG and RFID for hand assistive application," pp. 3537-3542, 2016.

[32] M. A. Diftler *et al.*, "RoboGlove A Grasp Assist Device for Earth and Space.," *In Proceedings of the 45th International Conference on Environmental Systems Bellevue, DC, USA, 12–16 July 2015,* 2015.

[33] H. C. Fischer, K. Stubblefield, T. Kline, X. Luo, R. V. Kenyon, and D. G. Kamper, "Hand Rehabilitation Following Stroke: A Pilot Study of Assisted Finger Extension Training in a Virtual Environment," *Topics in Stroke Rehabilitation,* vol. 14, no. 1, pp. 1-12, 2007/01/01 2007.

[34] H. K. Yap *et al.*, "A Fully Fabric-Based Bidirectional Soft Robotic Glove for Assistance and Rehabilitation of Hand Impaired Patients," *IEEE Robotics and Automation Letters,* vol. 2, no. 3, pp. 1383-1390, 2017.

[35] Y. Park, I. Jo, J. J. I. R. I. C. o. I. R. Bae, and Systems, "Development of a dual-cable hand exoskeleton system for virtual reality," pp. 1019-1024, 2016.

[36] B. W. K. Ang, C.-H. J. I. R. I. C. o. I. R. Yeow, and Systems, "Print-it-Yourself (PIY) glove: A fully 3D printed soft robotic hand rehabilitative and assistive exoskeleton for stroke patients," pp. 1219-1223, 2017.

[37] B. B. Kang, H. Choi, H. Lee, and K. J. Cho, "Exo-Glove Poly II: A Polymer-Based Soft Wearable Robot for the Hand with a Tendon-Driven Actuation System," (in eng), *Soft Robot,* vol. 6, no. 2, pp. 214-227, Apr 2019.

[38] D. Popov, I. Gaponov, and J.-H. J. I. A. T. o. M. Ryu, "Portable Exoskeleton Glove With Soft Structure for Hand Assistance in Activities of Daily Living," vol. 22, pp. 865-875, 2017.

[39] L. Randazzo, I. Iturrate, S. Perdikis, and J. d. R. Millán, "mano: A Wearable Hand Exoskeleton for

Activities of Daily Living and Neurorehabilitation," *IEEE Robotics and Automation Letters,* vol. 3, no. 1, pp. 500-507, 2018.

[40] K. O. Thielbar *et al.*, "Training finger individuation with a mechatronic-virtual reality system leads to improved fine motor control post-stroke," (in eng), *J Neuroeng Rehabil,* vol. 11, p. 171, Dec 26 2014.

[41] M. C. H. Chua, J. H. Lim, and R. C. H. Yeow, "Design and Characterization of a Soft Robotic Therapeutic Glove for Rheumatoid Arthritis," *Assistive Technology,* vol. 31, no. 1, pp. 44-52, 2019/01/01 2019.

[42] M. Li *et al.*, "An Attention-Controlled Hand Exoskeleton for the Rehabilitation of Finger Extension and Flexion Using a Rigid-Soft Combined Mechanism," (in eng), *Front Neurorobot,* vol. 13, p. 34, 2019.

[43] T. Bützer, O. Lambercy, J. Arata, and R. Gassert, "Fully Wearable Actuated Soft Exoskeleton for Grasping Assistance in Everyday Activities," (in eng), *Soft Robot,* vol. 8, no. 2, pp. 128-143, Apr 2021.

[44] Q. Meng, Z. Shen, Z. Nie, Q. Meng, Z. Wu, and H. Yu, "Modeling and Evaluation of a Novel Hybrid-Driven Compliant Hand Exoskeleton Based on Human-Machine Coupling Model," *Applied Sciences*, vol. 11, no. 22. doi: 10.3390/app112210825

[45] Z. Q. Tang, H. L. Heung, X. Q. Shi, R. K. Y. Tong, and Z. Li, "Probabilistic Model-Based Learning Control of a Soft Pneumatic Glove for Hand Rehabilitation," (in eng), *IEEE Trans Biomed Eng,* vol. 69, no. 2, pp. 1016-1028, Feb 2022.

[46] M. Sierotowicz *et al.*, "EMG-Driven Machine Learning Control of a Soft Glove for Grasping Assistance and Rehabilitation," *IEEE Robotics and Automation Letters,* vol. 7, no. 2, pp. 1566-1573, 2022.

[47] H. Taheri *et al.*, "Design and preliminary evaluation of the FINGER rehabilitation robot: controlling challenge and quantifying finger individuation during musical computer game play," (in eng), *J Neuroeng Rehabil,* vol. 11, p. 10, Feb 4 2014.

[48] R. Rätz, F. Conti, R. M. Müri, and L. Marchal-Crespo, "A Novel Clinical-Driven Design for Robotic Hand Rehabilitation: Combining Sensory Training, Effortless Setup, and Large Range of Motion in a Palmar Device," (in eng), *Front Neurorobot,* vol. 15, p. 748196, 2021.

[49] Z. Ma and P. Ben-Tzvi, "Design and Optimization of a Five-Finger Haptic Glove Mechanism," *Journal of Mechanisms and Robotics,* vol. 7, no. 4, 2015.

[50] E. A. Susanto, T. R. K. Y., and N. S. K. and Ho, "Hand exoskeleton robot for assessing hand and finger motor impairment after stroke," *HKIE Transactions,* vol. 22, no. 2, pp. 78-87, 2015/04/03 2015.

[51] Q. Bi, C.-J. Yang, X.-L. Deng, and J.-C. Fan, "Human finger mechanical impedance modeling: Using multiplicative uncertain model," vol. 230, no. 12, pp. 1978-1986, 2016.

[52] H. K. Yap, L. Jeong Hoon, F. Nasrallah, J. C. H. Goh, and R. C. H. Yeow, "A soft exoskeleton for hand assistive and rehabilitation application using pneumatic actuators with variable stiffness," in *2015 IEEE International Conference on Robotics and Automation (ICRA)*, 2015, pp. 4967-4972.

[53] S. C. Chapra, *Applied Numerical Methods With Matlab For Engineers And Scıentısts*. USA: McGraw-Hill Companies, 2012.

[54] S. W. Lee, K. A. Landers, and H. S. Park, "Development of a Biomimetic Hand Exotendon Device (BiomHED) for Restoration of Functional Hand Movement Post-Stroke," *IEEE Transactions on Neural Systems and Rehabilitation Engineering,* vol. 22, no. 4, pp. 886-898, 2014.

[55] H. In, B. B. Kang, M. Sin, and K. J. Cho, "Exo-Glove: A Wearable Robot for the Hand with a Soft Tendon Routing System," *IEEE Robotics & Automation Magazine,* vol. 22, no. 1, pp. 97-105, 2015.

[56] J. Yang, H. Xie, and J. Shi, "A novel motion-coupling design for a jointless tendon-driven finger exoskeleton for rehabilitation," *Mechanism and Machine Theory,* vol. 99, pp. 83-102, 2016/05/01/ 2016.

[57] D. Lau, D. Oetomo, and S. K. Halgamuge, "Generalized Modeling of Multilink Cable-Driven Manipulators With Arbitrary Routing Using the Cable-Routing Matrix," *IEEE Transactions on Robotics,* vol. 29, no. 5, pp. 1102-1113, 2013.

[58] Y. Hasegawa and T. Suzuki, "Thin and active fixture to hold finger for easy attachment and comfort of grasping support exoskeleton," in *2015 IEEE International Conference on Robotics and Automation*

(ICRA), 2015, pp. 4973-4978.

[59] E. Thompson-Bean, O. Steiner, and A. McDaid, "A soft robotic exoskeleton utilizing granular jamming," in *2015 IEEE International Conference on Advanced Intelligent Mechatronics (AIM)*, 2015, pp. 165-170.

[60] R. Kabir, M. S. H. Sunny, H. U. Ahmed, and M. H. Rahman, "Hand Rehabilitation Devices: A Comprehensive Systematic Review," vol. 13, no. 7, p. 1033, 2022.

[61] W. Widhiada, T. G. Nindhia, and N. Budiarsa, "Robust Control for the Motion Five Fingered Robot Gripper," *International Journal of Mechanical Engineering and Robotics Research,* vol. 4, pp. 226-232, 2015.

[62] J. Baek, M. Jin, and S. Han, "A New Adaptive Sliding-Mode Control Scheme for Application to Robot Manipulators," *IEEE Transactions on Industrial Electronics,* vol. 63, no. 6, pp. 3628-3637, 2016.

[63] Y. B. Shtessel, J. A. Moreno, and L. M. Fridman, "Twisting sliding mode control with adaptation: Lyapunov design, methodology and application," *Automatica,* vol. 75, pp. 229-235, 2017/01/01/ 2017.

[64] A. Wege and G. Hommel, "Development and control of a hand exoskeleton for rehabilitation of hand injuries," in *2005 IEEE/RSJ International Conference on Intelligent Robots and Systems*, 2005, pp. 3046-3051.

[65] A. Jalali, F. Piltan, A. Gavahian, M. Jalali, and MozhdehAdibi, "Model-Free Adaptive Fuzzy Sliding Mode Controller Optimized by Particle Swarm for Robot Manipulator," (in English), *International Journal of Information Engineering and Electronic Business,* vol. 5, no. 1, pp. 68-78, May 2013 2013.

[66] K. Hu, Z. Ma, S. Zou, J. Li, and H. Ding, "Impedance Sliding-Mode Control Based on Stiffness Scheduling for Rehabilitation Robot Systems," (in eng), *Cyborg Bionic Syst,* vol. 5, p. 0099, 2024.

[67] A. Lince, "ReHand - a portable assistive rehabilitation hand exoskeleton," Doctor of Philosophy Thesis Mechanical, Politecnico di Torino 2016.

[68] K. Serbest, "El Kaslarının Rehabilitasyonu İçin Aktif Dinamik El – El Bileği Ortezi Tasarımı. ," Doktora Tezi, Sakarya Üniversitesi Fen Bilimleri Enstitüsü, 2017.

[69] C.-H. Chen, D. S. Naidu, and M. P. Schoen, "Adaptive control for a five-fingered prosthetic hand with unknown mass and inertia," vol. 10, no. 5 .J WTOS, pp. 148–161, 2011.

[70] M. Marul, "Development of a dynamically controlled robot for hand-wrist rehabilitation," Ph.D, Institute of Science, Karadeniz Technical University, Türkiye, 2024.

[71] H. Wang *et al.*, "Adaptive Integral Terminal Sliding Mode Control for Automobile Electronic Throttle via an Uncertainty Observer and Experimental Validation," *IEEE Transactions on Vehicular Technology,* vol. 67, no. 9, pp. 8129-8143, 2018.

[72] Y. Hu and H. Wang, "Robust tracking control for vehicle electronic throttle using adaptive dynamic sliding mode and extended state observer," *Mechanical Systems and Signal Processing,* vol. 135, p. 106375, 2020/01/01/ 2020.

[73] M. Doğan and Ü. Önen, "Trajectory tracking control of a two wheeled self-balancing robot by using sliding mode control," (in en), *Konya Journal of Engineering Sciences,* vol. 12, no. 3, pp. 652-670, September 2024.

[74] J.-J. Wang and G.-Y. Liu, "Hierarchical sliding-mode control of spatial inverted pendulum with heterogeneous comprehensive learning particle swarm optimization," *Information Sciences,* vol. 495, pp. 14-36, 2019/08/01/ 2019.

[75] J. J. Wang, "Stabilization and tracking control of X-Z inverted pendulum with sliding-mode control," (in eng), *ISA Trans,* vol. 51, no. 6, pp. 763-70, Nov 2012.

[76] J. Kennedy and R. Eberhart, "Particle swarm optimization," in *Proceedings of ICNN'95 - International Conference on Neural Networks*, 1995, vol. 4, pp. 1942-1948 vol.4.

[77] R. Storn and K. Price, "Differential Evolution – A Simple and Efficient Heuristic for global Optimization over Continuous Spaces," *Journal of Global Optimization,* vol. 11, no. 4, pp. 341-359, 1997/12/01 1997.